J. Fluid Mech. (1986), *vol.* 169, *pp.* 71–107
Printed in Great Britain

Unstable transition properties of the driven magnetohydrodynamic sheet pinch

By R. B. DAHLBURG,†
Department of Physics, College of William and Mary, Williamsburg, VA 23185

T. A. ZANG,
NASA Langley Research Center, Hampton, VA 23665

AND D. MONTGOMERY
Department of Physics and Astronomy, Dartmouth College, Hanover, NH 03755

(Received 10 June 1985 and in revised form 7 January 1986)

The unstable transition behaviour of a bounded, current-carrying, two-dimensional magnetofluid is explored, using the hydrodynamic theory developed for parallel shear flows as a guide. The time development of a perturbed driven magnetohydrodynamic sheet pinch is simulated numerically. The nonlinear partial differential equations of two-dimensional, incompressible, viscoresistive magnetohydrodynamics are advanced in time numerically by means of a semi-implicit, mixed Fourier collocation–finite difference algorithm. Nonlinear excitation of the higher wavenumbers results in the development of electric current sheets of finite extent, as well as the formation of 'attraction currents' centred at the magnetic O-points. A secondary instability mechanism, the dynamic tearing of the electric current sheet, is also observed. This dynamic tearing leads to sawtooth-like temporal oscillations in certain global quantities. The long time state of the system resembles a nonlinearly saturated state with significant excitation of many wavenumbers. Some features of this state can be understood by means of a Landau nonlinear stability theory based on certain assumptions about the perturbation energy balance.

1. Introduction

The magnetohydrodynamic sheet pinch is a two-dimensional field structure that is believed to approximate a wide variety of physical situations. It consists of a plane electric current layer in a static magnetofluid, across which a d.c. magnetic field changes sign. It is well known that this configuration can be unstable to perturbations in the velocity or magnetic fields (e.g. Furth, Killeen & Rosenbluth 1963). Finite resistivity allows the magnetic field topology to evolve into the magnetic X-point reconnection geometry (Dungey 1958). This rearrangement of the magnetic field is generally accompanied by a high-speed motion of the magnetofluid away from the magnetic X-point, indicating that some of the magnetic energy is being transformed into kinetic energy at the magnetic X-point. Large electric currents also develop in the region of the magnetic X-point, indicating that ohmic dissipation of the magnetic energy is significant in this region.

These features have led to the belief that magnetohydrodynamic (MHD) sheet

† Present address: Laboratory for Computational Physics, Naval Research Laboratory, Washington DC 20375.

pinch instabilities might be related to many, otherwise unexplained, physical phenomena. Solar physicists, for instance, hypothesize that MHD sheet pinch reconnection occurs during the evolution of solar flares, and perhaps produces a rapid ejection of charged particles (e.g. Sonnerup 1979; Forbes & Priest 1983). The fusion community has retained an interest in this configuration, since it may be thought of as a prototype for resistive instabilities of a kind thought to contribute to the breakdown of plasma confinement in many magnetic fusion devices, such as tokamaks (e.g. Bateman 1978; White 1983; Manheimer & Lashmore-Davies 1984).

One common feature of all such studies is that the theoretical effort has run far ahead of experimental measurement. The impossibility of performing solar physical and astrophysical 'experiments' is clear, while laboratory experiments dealing with magnetic reconnection have not been performed in the temperature regime where they could be adequately diagnosed (the remarkable work of Gekelman, Stenzel & Wild must be excepted (Wild, Gekelman & Stenzel 1981; Stenzel & Gekelman 1981; Gekelman & Stenzel 1981; Gekelman, Stenzel & Wild 1982; Stenzel, Gekelman & Wild 1982, 1983).

Theoretical treatments have often been divided along disciplinary lines. In space physics magnetic reconnection has often been studied as a steady state phenomenon (e.g. Vasyliunas 1975; Soward & Priest 1977), while the fusion community has looked at it as a temporally evolving instability. We shall adopt the latter point of view, and henceforth limit the discussion to this case.

The inherent complexity of the magnetic reconnection process renders analysis difficult, so that it is a common practice first to simplify in some way the equations which govern the behaviour of the system. By far the most widespread technique is to linearize the governing equations, and then to attack the instability problem by means of a normal mode analysis (Furth *et al.* 1963; Wesson 1966). The magnetofluid viscosity is customarily ignored in these analyses, but more recent investigations have shown its importance (Dahlburg *et al.* 1983; Bondeson & Sobel 1984).

Analytic theories dealing with the nonlinear properties of the unstable eigenmodes of the magnetohydrodynamic sheet pinch have been given by Rutherford (1973) and by White *et al.* (1977). These analyses assume that the viscous dissipation and magnetofluid inertia are negligible, and follow the evolution of a single eigenmode into the nonlinear regime. The exponential growth of the linear mode is predicted to slow nonlinearly into a phase of algebraic growth, followed by the nonlinear saturation of the mode. More recent analyses by Pao, Rosenau & Guo (1983), and Dahlburg (1985) have shown that viscous and inertial effects are important in determining the nonlinear rate of growth and the saturated amplitude of the perturbation.

In order to understand better such complex nonlinear processes, it is by now common to simulate by means of numerical methods the temporal evolution of the magnetofluid. Computations that have been performed of the nonlinear evolution of the perturbed magnetohydrodynamic sheet pinch have exhibited certain methodological differences, both in terms of the model and the numerical method employed. Schnack & Killeen (1979, 1980) employed a conservative finite difference scheme. Using an inviscid, compressible magnetofluid model, they followed the nonlinear evolution of eigenmodes of the linearized problem. They found a period of exponential growth, followed by nonlinear saturation of the mode. They were particularly interested in determining the nonlinear effects on the topology of the magnetic field. Matthaeus & Montgomery (1981) employed a Fourier spectral (Galerkin truncation)

method in space. They considered a viscoresistive, incompressible magnetofluid in a periodic box. Two electric current sheets of opposite sign were present in the computational box. Small random perturbations were imposed initially on both the magnetic and velocity fields, and the system was allowed to evolve without any driving. As a result the ohmic decay of the electric current profile was significant during the course of their simulations. These authors focused on the nonlinear behaviour of the electric current density, which emphasizes the excitation of the high wavenumber components of the magnetic field. They found that localized current structures, which they called filaments, would develop in the vicinity of the magnetic X-point. This localization indicated that many of the high wavenumber components of the magnetic field were excited, a feature indicative of turbulent behaviour. Subsequently, Matthaeus (1982) reported a related result for the magnetofluid vorticity.

It is by now well known that magnetofluids exhibit a tendency to become excited at very small spatial scales due to the nonlinearities in the governing equations (Fyfe, Montgomery & Joyce 1977; Pouquet 1978; Orszag & Tang 1979). In order to simulate accurately the behaviour of a magnetofluid, it is necessary to resolve all of the spatial scales which are excited. The extent of the high wavenumber spectrum is determined by the magnitude of the dissipation coefficients. The number of spatial scales retained is also limited by the computational resources which are available. Combining these two criteria, we have the result that the present generation of computers, which includes the CDC CYBER 205 and the CRAY-XMP, allows the simulation of adequately resolved two-dimensional magnetofluids with Lundquist numbers no greater than approximately 1000 (e.g. Matthaeus & Lamkin 1985). Note that for the MHD sheet pinch this parameter regime is linearly unstable for electric current profiles of interest (Dahlburg *et al.* 1983).

Low values of the resistive Lundquist number have a serious consequence for pure decay simulations of the magnetohydrodynamic sheet pinch (Matthaeus & Montgomery 1981; Matthaeus 1982), namely the mean magnetic field decays rapidly as a function of time. The rapidity of this ohmic decay of the mean magnetic field implies that the evolution of the perturbations is affected significantly, since the exchange of energy between the mean magnetic field and the perturbed fields depends on the form of the mean magnetic field. All of the interesting dynamical events are seen to occur in ten to twenty Alfvén transit times.

In this paper the decay of the mean magnetic field is opposed by a constant external electric field. This allows us to use a low enough value of the resistive Lundquist number to ensure adequate resolution and yet not have the evolution of the system dominated by the ohmic decay of the mean magnetic field. For the case of arbitrary infinitesimal initial perturbations, alterations in the mean magnetic field will only occur when these perturbations attain finite amplitude. The external driving also ensures that the long time state of the system will be non-trivial. For instance, a state of secondary equilibrium is possible, in which the amount of energy injected into the system would be equal to the amount of energy dissipated.

While the previous paragraphs have emphasized the importance of ohmic dissipation in the problem, it must be stressed that viscous dissipation also plays a role. It is a common practice in the literature to ignore this process in the analysis of MHD sheet pinch instabilities (Furth *et al.* 1963; Rutherford 1973; White *et al.* 1977; Schnack & Killeen 1979, 1980). By kinetic theory estimates, however, the viscosity is of at least the same order of magnitude as the magnetic diffusivity in plasmas of interest (cf. Braginskii 1965). Viscous dissipation will be especially significant in

regions of high vorticity, and just such regions are known to develop in the vicinity of magnetic X-points (Matthaeus 1982). Hence, assuming that the magnetofluid is inviscid will lead to an incomplete picture of the magnetic X-point dynamics. This is important when considering the possibility of a saturated state, for in that state the energy injected is balanced by the dissipated energy.

Finally the nature of the perturbations must be discussed. To simplify the analytic problem it is common to consider single-mode perturbations on prescribed laminar equilibria (Furth *et al.* 1963; Rutherford 1973; White *et al.* 1977). It is, however, doubtful that such equilibria are ever accurately achieved within any fusion confinement device. Furthermore, the irregular character of the startup phase in such devices virtually guarantees that the existing perturbations are extremely complex. We can represent this situation somewhat by using a moderately high level of random noise in the magnetic and velocity fields as the initial perturbations. The initial activation of many wavenumbers in both fields ensures that larger regions of phase space are accessible to the system than are allowed by single eigenmode perturbations. As will be seen, the system executes a different evolution than that predicted by a single mode analysis.

We report here on numerical simulations of the nonlinear evolution of the driven magnetohydrodynamic sheet pinch. We have formulated the problem in such a way that the large amount of theory and techniques that have been developed for the study of stability and transition in parallel shear flows can be utilized. The geometric situation is that characteristic of plane Poiseuille or plane Couette flow, namely the magnetofluid is confined between two infinite parallel plates. Periodicity of the magnetofluid in the coordinates parallel to the walls is assumed to render the problem tractable. An incompressible, viscoresistive, two-dimensional magnetofluid model is used. The decay of the mean magnetic profile is opposed by a constant, external electric field. The initial perturbations in the magnetic and velocity fields are in general random (although cases with eigenmode initial conditions are considered). A mixed Fourier collocation–finite difference algorithm with a semi-implicit temporal differencing scheme based on the algorithm of Moin & Kim (1982) is used to advance the system in time.

The presence of an electric field allows us to investigate the long time state of the driven system and the processes by which it is achieved. The nonlinear evolution of this driven system is seen to exhibit rather different behaviour than the pure decay case. The maximum nonlinearity is seen during the coalescence of the magnetic islands which arise spontaneously in the evolution of the system. A secondary instability, the dynamic tearing of the electric current sheet, is observed, as is the formation of nonlinear 'attraction currents' centred on the magnetic 0-points. The long time state of the system resembles a nonlinear saturation of the initial disturbance with many of the systems' wavenumbers being excited.

The governing equations, geometry, and initial equilibrium state of the system are described in §2. The computational procedure is described in §3, as are the diagnostics. Representative computational results are reported in §4. A model for the nonlinear evolution of supercritical linear instabilities in the vicinity of the neutral stability boundary is given in §5. The predictions of this model are compared with numerical simulation. The results are discussed in §6.

2. Formulation of the problem

The magnetofluid under consideration is confined between parallel, rigid, impenetrable plates. The plates are regarded as perfect conductors coated with a thin layer of insulating material. This boundary permits the entrance of magnetic flux to drive the system (Montgomery 1984). No-slip boundary conditions are imposed on the viscous magnetofluid at the walls. The normal component of the magnetic field is constrained to equal zero at the walls, but the tangential component of the electric current is unrestricted. The x-direction is regarded as periodic, while all variation in y is ignored.

The evolution of an incompressible magnetofluid is governed by the following equations, written in a dimensionless form (e.g. Montgomery 1984):

$$\frac{\partial u}{\partial t}-w\left(\frac{\partial w}{\partial x}-\frac{\partial u}{\partial z}\right)=-\frac{\partial \Pi}{\partial x}-\frac{\partial A}{\partial x}\nabla^2 A+\nu\nabla^2 u, \tag{2.1a}$$

$$\frac{\partial w}{\partial t}+u\left(\frac{\partial w}{\partial x}-\frac{\partial u}{\partial z}\right)=-\frac{\partial \Pi}{\partial z}-\frac{\partial A}{\partial z}\nabla^2 A+\nu\nabla^2 w, \tag{2.1b}$$

$$\frac{\partial u}{\partial x}+\frac{\partial w}{\partial z}=0, \tag{2.1c}$$

$$\frac{\partial A}{\partial t}+u\frac{\partial A}{\partial x}+w\frac{\partial A}{\partial z}=\eta(z)\nabla^2 A+E, \tag{2.1d}$$

where

$\boldsymbol{v}(x,z,t)$ = magnetofluid velocity = $(u(x,z,t),0,w(x,z,t))$,

$\Pi(x,z,t)=p+\frac{1}{2}u^2+\frac{1}{2}w^2$ = total fluid pressure,

$p(x,z,t)$ = mechanical pressure/mass density,

$\boldsymbol{A}(x,z,t)$ = magnetic vector potential = $A\hat{e}_y$,

ν = kinematic viscosity,

$\eta(z)=\eta(z=0)\left(\left.\frac{\mathrm{d}^2A_0}{\mathrm{d}z^2}\right|_{z=0}\right)\left(\frac{\mathrm{d}^2A_0}{\mathrm{d}z^2}\right)^{-1}$ = dimensionless resistivity profile,

$E=-\eta(z=0)\left.\frac{\mathrm{d}^2A_0}{\mathrm{d}z^2}\right|_{z=0}$ = constant, externally applied electric field,

$A_0(z)$ = initial mean magnetic vector potential.

Unit mass density is assumed.

The following terms are also of importance:

$\omega(x,z,t)=(\nabla\times\boldsymbol{v})_y$ = magnetofluid vorticity,

$\boldsymbol{B}(x,z,t)=\nabla\times A\hat{e}_y$ = magnetic field = $(B_x(x,z,t),0,B_z(x,z,t))$,

$J(x,z,t)=-\nabla^2 A$ = electric current density,

$S=\dfrac{1}{\eta(z=0)}$ = resistive Lundquist number,

$M=\dfrac{1}{\nu}$ = viscous Lundquist number.

This specification of E and $\eta(z)$ allows the system to maintain the unperturbed equilibrium (Furth *et al.* 1963; Waddell *et al.* 1976). In addition, it simulates the

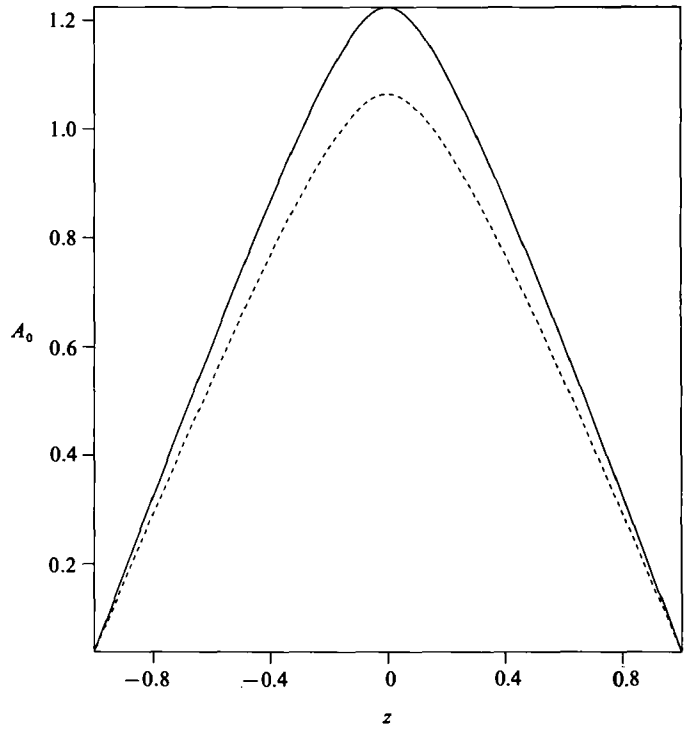

FIGURE 1. Run D; mean magnetic vector potential. Solid line, $t = 0$; dashed line, $t = 161.009$.

frequent experimental feature of a higher interior electrical conductivity profile, which in turn is due to higher temperatures. The electrical conductivity profile is, however, assumed to be temporally constant.

The confining plates are regarded as perfect conductors coated with a thin layer of insulating dielectric. In the dimensionless units, the magnetic vector potential boundary condition becomes

$$A(z = 1) = A(z = -1) = \text{Constant}, \tag{2.2}$$

independent of time.

The tangential electric current at the walls is unrestrained.

No-slip boundary conditions are imposed on the velocity field of the viscous magnetofluid:

$$u(z = 1) = u(z = -1) = 0, \quad w(z = 1) = w(z = -1) = 0. \tag{2.3a, b}$$

We choose an initial mean magnetic field which gives a sheet pinch-like field configuration. The initial mean magnetic vector potential is

$$A_0(z) = -z \tan^{-1}\gamma z + \frac{1}{2\gamma} \ln\left(\frac{1+\gamma^2 z^2}{1+\gamma^2}\right) + \tan^{-1}\gamma + \frac{\gamma}{S}, \tag{2.4}$$

with the corresponding mean magnetic field

$$B_0(z) = \tan^{-1}\gamma z, \tag{2.5}$$

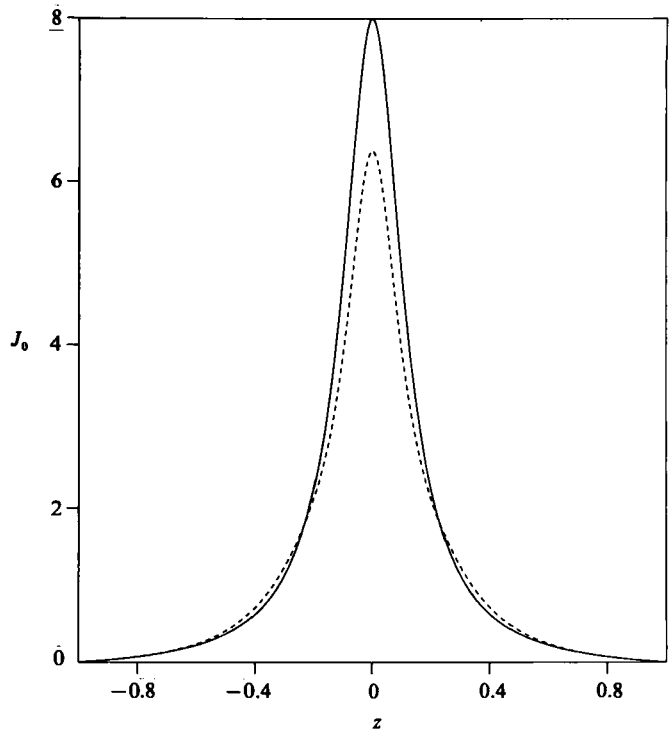

FIGURE 2. Run D; mean electric current density. Solid line, $t = 0$; dashed line, $t = 161.009$.

and the corresponding mean electric current density

$$J_0(z) = \gamma(1+\gamma^2 z^2)^{-1}, \tag{2.6}$$

where γ may be thought of as a 'stretching parameter' (Dahlburg *et al.* 1983). The mean fluid velocity is zero. This choice of mean fields gives a configuration in which there exists an infinite plane electric current layer with a magnetic field changing sign across it. The initial mean magnetic vector potential for the case $\gamma = 8$, $M = S = 200$ is shown in figure 1. The corresponding initial mean electric current density is shown in figure 2. This case will be discussed at length in §4, so it is useful to know certain other physically relevant parameters. For this case the initial mean $\langle B_0^2 \rangle$ is equal to 19.001. For this mean magnetic field and unit mass density the Alfvén speed is equal to 1.23. If the characteristic length is taken to be the half-channel width, then the initial Alfvén transit time equals $1/1.23 = 0.813$. The electric field in this case reduces to $E = \gamma/S = 0.04$.

Random perturbations are imposed initially on both the magnetic and velocity fields, and the perturbed system is then allowed to evolve in time. The total initial magnetic vector potential is given by

$$A(x,z,t=0) = A_0(z) + \epsilon \sum_n \sum_m [(A_{mn}\cos mx + B_{mn}\sin mx)\cos(\tfrac{1}{2}n\pi z) + (C_{mn}\cos mx + D_{mn}\sin mx)\sin(\tfrac{1}{2}(n+1)\pi z)], \tag{2.7}$$

where $m = 1,2,3,\ldots,m_{\max}$; $n = 1,3,5,\ldots,n_{\max}$; $\epsilon \ll 1$; A_{mn}, B_{mn}, C_{mn}, D_{mn} = random real numbers with zero mean and unit variance.

The initial stream function is expressed in terms of Chandrasekhar–Reid functions (Chandrasekhar 1961) as

$$\psi(x,z,t=0) = \epsilon \sum_n \sum_m \Big[(Q_{mn}\cos mx + R_{mn}\sin mx)\Big(\frac{\cosh\lambda_n z}{\cosh\lambda_n} - \frac{\cos\lambda_n z}{\cos\lambda_n}\Big) + (S_{mn}\cos mx + T_{mn}\sin mx)\Big(\frac{\sinh\mu_n z}{\sinh\mu_n} - \frac{\sin\mu_n z}{\sin\mu_n}\Big)\Big], \quad (2.8)$$

where $m = 1,2,3,\ldots,m_{\max}$; $n = 1,2,3,\ldots,n_{\max}$; $\epsilon \ll 1$; $Q_{mn}, R_{mn}, S_{mn}, T_{mn}$ = random real numbers with zero mean and unit variance; λ_n = positive roots of $(\tanh\lambda + \tan\lambda = 0)$; μ_n = positive roots of $(\coth\mu - \cot\mu = 0)$; and:

$$u(x,z,t) = -\frac{\partial\psi}{\partial z}; \quad w(x,z,t) = \frac{\partial\psi}{\partial x}.$$

3. Computational procedure

The numerical method used to solve the governing equations is based on the algorithm developed by Moin & Kim (1982) for the study of parallel shear flows. The equations to be advanced temporally, i.e. equations (2.1*a*) to (2.1*d*), are written in the rotation form. The spatially discrete and time continuous version of the ideal form of these equations conserves energy exactly. As a consequence of the energy conservation property, writing the equations in this form leads to enhanced stability for the numerical method.

The x-direction, which is regarded as periodic, is naturally discretized by the Fourier collocation method (Gottlieb & Orszag 1977). All nonlinear product terms are evaluated most conveniently in configuration space. The x derivatives are evaluated in Fourier space without phase error. Most of the z derivatives are discretized by second-order central differences on a stretched grid. The difference formulae are obtained by differentiating the second-order Lagrange interpolating polynomial an appropriate number of times, and then evaluating the resulting expression at the central grid point. The z derivative term in the continuity equation (2.1*c*) is evaluated by a first-order finite difference discretization.

A staggered mesh in the z-direction is used for the velocity, pressure, and magnetic vector potential values. The pressure is defined at the cell centres, ζ, which are given by

$$\zeta_{k-\frac{1}{2}} = -\cos\Big[\frac{(k-\frac{1}{2})\pi}{k_{\max}}\Big]\Big|\cos\Big[\frac{(k-\frac{1}{2})\pi}{k_{\max}}\Big]\Big|, \quad (3.1)$$

where $k = 1,2,3,\ldots,k_{\max}$. The velocity and magnetic vector potential are defined at the cell edges of the staggered mesh, which are given by

$$\left.\begin{aligned} z_0 &= -1.0, \\ z_k &= \tfrac{1}{2}(\zeta_{k-\frac{1}{2}} + \zeta_{k+\frac{1}{2}}); \quad k = 1,2,3,\ldots,k_{\max}-1, \\ z_{k_{\max}} &= 1.0. \end{aligned}\right\} \quad (3.2)$$

The mesh is constructed so as to augment the numerical resolution in the central region and at the walls of the channel.

A semi-implicit temporal discretization is employed. All nonlinear terms and the parallel diffusion terms are advanced explicitly in time by the second-order Adams–Bashforth method. The vertical diffusion terms are advanced implicitly in time by

the Crank–Nicolson method. Terms involving the pressure are advanced implicitly in time by the backward Euler method. The incompressibility of the magnetofluid is enforced implicitly.

To illustrate better the method, first collect the terms to be advanced explicitly:

$$\left.\begin{aligned} H_1 &\equiv w\left(\frac{\partial w}{\partial x}-\frac{\partial u}{\partial z}\right)-\frac{\partial A}{\partial x}\nabla^2 A+\nu\frac{\partial^2 u}{\partial x^2},\\ H_3 &\equiv -u\left(\frac{\partial w}{\partial x}-\frac{\partial u}{\partial z}\right)-\frac{\partial A}{\partial z}\nabla^2 A+\nu\frac{\partial^2 w}{\partial x^2},\\ H_4 &\equiv -u\frac{\partial A}{\partial x}-w\frac{\partial A}{\partial z}+\eta(z)\frac{\partial^2 A}{\partial x^2}+E. \end{aligned}\right\} \tag{3.3}$$

Substitute these expressions into the governing equations, and then discretize the system in time:

$$\left.\begin{aligned} u^{n+1} &= u^n-\Delta t\left(\frac{\partial \Pi}{\partial x}\right)^{n+1}+\tfrac{1}{2}\Delta t\,[3H_1^n-H_1^{n-1}]+\tfrac{1}{2}\nu\Delta t\left[\left(\frac{\partial^2 u}{\partial z^2}\right)^{n+1}+\left(\frac{\partial^2 u}{\partial z^2}\right)^n\right],\\ w^{n+1} &= w^n-\Delta t\left(\frac{\partial \Pi}{\partial z}\right)^{n+1}+\tfrac{1}{2}\Delta t\,[3H_3^n-H_3^{n-1}]+\tfrac{1}{2}\nu\Delta t\left[\left(\frac{\partial^2 w}{\partial z^2}\right)^{n+1}+\left(\frac{\partial^2 w}{\partial z^2}\right)^n\right],\\ \left(\frac{\partial^2 u}{\partial x^2}\right)^{n+1}&+\left(\frac{\partial^2 w}{\partial z^2}\right)^{n+1}=0,\\ A^{n+1} &= A^n+\tfrac{1}{2}\Delta t\,[3H_4^n-H_4^{n-1}]+\tfrac{1}{2}\eta(z)\,\Delta t\left[\left(\frac{\partial^2 A}{\partial z^2}\right)^{n+1}+\left(\frac{\partial^2 A}{\partial z^2}\right)^n\right], \end{aligned}\right\} \tag{3.4}$$

where Δt is defined to be the size of the time step, and the superscript n indexes the time level.

This system of partial differential equations is Fourier transformed in x, resulting in a set of ordinary differential equations in z for each value of the x wavenumber k_x:

$$\tilde{u}^{n+1}+ik_x\Delta t\tilde{\Pi}^{n+1}-\frac{\nu\Delta t}{2}\left(\frac{\partial^2\tilde{u}}{\partial z^2}\right)^{n+1}=\tilde{Q}_1^n, \tag{3.5a}$$

$$\tilde{w}^{n+1}+\Delta t\left(\frac{\partial\tilde{\Pi}}{\partial z}\right)^{n+1}-\frac{\nu\Delta t}{2}\left(\frac{\partial^2\tilde{w}}{\partial z^2}\right)^{n+1}=\tilde{Q}_3^n, \tag{3.5b}$$

$$ik_x\tilde{u}^{n+1}+\left(\frac{\partial\tilde{w}}{\partial z}\right)^{n+1}=0, \tag{3.5c}$$

$$\tilde{A}^{n-1}-\frac{\eta(z)\,\Delta t}{2}\left(\frac{\partial^2\tilde{A}}{\partial z^2}\right)^{n+1}=\tilde{Q}_4^n, \tag{3.5d}$$

where the tildes denote one-dimensional, Fourier transformed quantities. The functions $\tilde{Q}_i^n$ represent terms involving the pressure, velocity field, magnetic field, and electric field at time steps n and $n-1$.

Equations (3.5a,b,d) are evaluated at the cell edges, and equation (3.5c) is evaluated at the cell centres. When this system of equations is discretized in z an algebraic system of equations in block tridiagonal form for the Fourier transformed field variables results. This system of equations can be inverted by conventional methods.

Periodic boundary conditions in x on all field variables are built into the algorithm.

No-slip boundary conditions are imposed on the velocity field at the walls at $z = 1$ and $z = -1$:

$$u(z_0) = u(z_{k_{\max}}) = 0, \quad w(z_0) = w(z_{k_{\max}}) = 0. \tag{3.6a, b}$$

The normal component of the magnetic field is constrained to equal zero at the walls, i.e.

$$A(z_0) = A(z_{k_{\max}}) = \text{Constant}. \tag{3.7}$$

The tangential electric current at the walls remains constant to about four significant digits, although this boundary condition is not explicitly enforced. Because of the use of the staggered grid, boundary conditions on the pressure term at the wall are unnecessary and hence are not imposed (Harlow & Welch 1965).

The following diagnostics are employed to follow the evolution of the system. Contour plots of the magnetic vector potential, the electric current density, the velocity stream function, and the vorticity of the magnetofluid, exhibit structures which occur during the evolution of the computed fields. The contours which are plotted represent equal increments of magnitude over the range of values of the field. Note that in two dimensions contours of constant magnetic vector potential are equivalent to magnetic field lines. Plots of the mean magnetic vector potential and the mean electric current density are also useful diagnostics, since they show the deformations in these fields due to the action of the nonlinear terms.

Certain global quantities are also useful in following the evolution of the system:

Mean magnetic energy:

$$\frac{1}{2}\int_0^{2\pi}\int_{-1}^{1} |B_0(z,t)\,\hat{e}_x|^2\,\mathrm{d}x\,\mathrm{d}z,$$

Perturbed magnetic energy:

$$\frac{1}{2}\int_0^{2\pi}\int_{-1}^{1} |\boldsymbol{B}(x,z,t) - B_0(z,t)\,\hat{e}_x|^2\,\mathrm{d}x\,\mathrm{d}z,$$

Kinetic energy:

$$\frac{1}{2}\int_0^{2\pi}\int_{-1}^{1} |\boldsymbol{v}(x,z,t)|^2\,\mathrm{d}x\,\mathrm{d}z,$$

One-dimensional modal magnetic energy:

$$\frac{1}{2}\int_{-1}^{1} |\boldsymbol{B}(k_x,z,t)|^2\,\mathrm{d}z,$$

One-dimensional modal kinetic energy:

$$\frac{1}{2}\int_{-1}^{1} |\boldsymbol{v}(k_x,z,t)|^2\,\mathrm{d}z,$$

where $B_0(z,t)\,\hat{e}_x$ is defined to be the mean magnetic field ($= \boldsymbol{B}(k_x = 0, z, t)$), $\boldsymbol{B}(k_x, z, t)$ is the one-dimensional Fourier transformed magnetic field, and $\boldsymbol{v}(k_x, z, t)$ is the one-dimensional Fourier transformed velocity field. In the plots, the configuration space global quantities are area averaged to facilitate comparison with the one-dimensional modal energies.

An obvious test of the computer code is its ability to simulate correctly the evolution of the linearly unstable modes. This can be achieved by initializing it with small enough doses of the eigenfunctions that the effect of the nonlinear terms is relatively insignificant. As a test case, we consider $B_0(z) = \arctan(8z)$, $M = S = 100$,

and with the parallel wavenumber of the disturbance equal to one. For this case the growth rate of the unstable eigenmode is found to equal 0.1822 (a more detailed discussion of the linearized problem is presented in §5). Details of this validation run are given in table 1, where it is called run A. The timestep used throughout equals 0.007 854. From the computer perturbed energies, linear growth rates can be calculated and compared with the result predicted by the linear theory. The change in kinetic energy implies a velocity field growth rate equal to 0.1815, which differs from the predicted value by 0.384 %. The change in perturbed magnetic energy implies a perturbed magnetic field growth rate equal to 0.1816, which differs from the predicted value by 0.329 %. At the conclusion of run A the mean magnetic energy is 99.995 % of its initial value, indicating that deformation of the mean magnetic profile is insignificant and hence that the nonlinear terms in the governing equations have not been excited significantly.

A second validation run of the same kind is listed in table 1 as run F. In this run the same initial mean magnetic field is used, but the Lundquist numbers are increased to 200. The parallel wavenumber of the linear disturbance is equal to two. For this case the unstable eigenmode has a growth rate equal to 0.252 (see table 3). The same timestep is used as in run A. For this case the change in kinetic energy implies a velocity field growth rate of 0.251, which differs from the predicted value by 0.397 %. The change in the perturbed magnetic energy implies a perturbed magnetic field growth rate of 0.251, which is in error by the same amount. At the conclusion of this run the mean magnetic energy is 99.997 % of its initial value.

4. Evolution from random initial conditions

Data for the runs performed is given in table 1. We describe here in detail case D, which exhibits all of the essential features found in the other runs. The timestep equals 0.001 963 5 initially and is subsequently reduced as necessary in order that the CFL condition be satisfied. The initial perturbations are given in (2.7) and (2.8), with:

$$A\colon n_{\max} = 8; \quad m_{\max} = 8; \quad \epsilon = 0.002,$$

$$\psi\colon n_{\max} = 7; \quad m_{\max} = 16; \quad \epsilon = 0.002.$$

The initial size of the perturbed fields relative to the mean magnetic field can be determined in a global sense by a comparison of the initial values of the various energies (see table 2), where the perturbed energies are defined as having no mean part. It is seen that the perturbed magnetic energy is initially 0.0278 % of the mean magnetic energy, and that the kinetic energy is initially 0.0292 % of the mean magnetic energy. Figure 1 shows the initial mean magnetic vector potential profile, and figure 2 shows the initial mean electric current density profile. Figures 3 to 6 are contour plots of, respectively, the initial magnetic vector potential, the initial electric current density, the initial velocity stream function, and the initial vorticity of the magnetofluid.

The initial phase of the system's evolution is characterized by an extremely rapid net loss of perturbed energy, both magnetic and kinetic. This is perhaps due to the decaying of the damped eigenmodes, or alternatively to the nonlinear transfer of excitations into the viscous and ohmic dissipation ranges. The mean magnetic energy remains relatively unchanged.

After this period a phase of growth ensues, with most of the growth being concentrated in the lower k_x velocity and magnetic modes. Figure 7 shows the perturbed energies as functions of time. The initial phase of rapid perturbed energy

Run	Perturbation type	M	S	$I \times K$	Initial mean magnetic energy	Initial perturbed magnetic energy	Initial kinetic energy	Final time	Final mean magnetic energy	Final perturbed magnetic energy	Final kinetic energy
A	Eigenmode ($\alpha = 1$)	100	100	4×129	0.75602	0.19828×10^{-8}	0.23335×10^{-8}	23.562	0.75598	0.10318×10^{-4}	0.12218×10^{-4}
B	Eigenmode ($\alpha = 1$)	100	100	32×129	0.75602	0.1980×10^{-4}	0.2330×10^{-4}	70.688	0.62970	0.5231×10^{-2}	0.1276×10^{-2}
C	Random	50	50	16×129	0.75602	0.22954×10^{-3}	0.20202×10^{-3}	47.12	0.59373	0.10620×10^{-1}	0.26984×10^{-2}
D	Random	200	200	64×129	0.75602	0.21026×10^{-3}	0.22076×10^{-3}	161.009	0.57189	0.63404×10^{-2}	0.16103×10^{-2}
E	Random	400	400	64×129	0.75602	0.21026×10^{-3}	0.22076×10^{-3}	58.906	0.60630	0.94989×10^{-2}	0.16339×10^{-2}
F	Eigenmode ($\alpha = 2$)	100	100	8×129	0.75602	0.22662×10^{-8}	0.91781×10^{-9}	15.708	0.75600	0.60549×10^{-5}	0.24404×10^{-5}
G	Eigenmode ($\alpha = 2$)	100	100	32×129	0.75602	0.16470×10^{-5}	0.84691×10^{-6}	62.832	0.62953	0.52284×10^{-2}	0.12272×10^{-2}

TABLE 1. Table of runs performed. $B_0(z, t = 0) = \arctan(8z)$, I = number of Fourier modes in x, K = number of grid points in z.

Time	0	15.708	31.416	161.009
Mean magnetic energy	0.75602	0.75402	0.67569	0.57189
Perturbed magnetic energy	0.21026×10^{-3}	0.44266×10^{-3}	0.99003×10^{-2}	0.63404×10^{-2}
Kinetic energy	0.22076×10^{-3}	0.16813×10^{-3}	0.30036×10^{-2}	0.16103×10^{-2}

TABLE 2. Energies at significant times during run D.

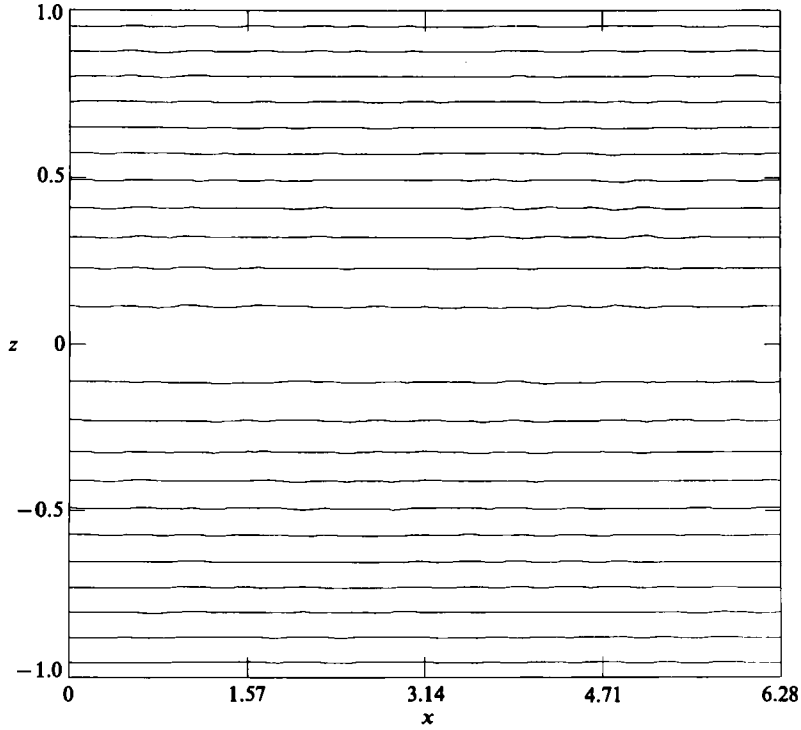

FIGURE 3. Run D; contour plot of magnetic vector potential at $t = 0$. The maximum contour value is 1.18. The minimum contour value is 0.0983.

loss is evident in these plots. Numerical solution of the linearized problem indicates that several of the lower k_x modes are linearly unstable, with the $k_x = 2$ eigenmode being the most unstable. The results of the eigenmode analysis are shown in table 3. In agreement with the linear theory, by this time in the run (approximately $t = 16$) the $k_x = 2$ magnetic and velocity modes exhibit the greatest enhancement. An inspection of the modal energy plots for the lower k_x magnetic and velocity modes, figures 8 and 9, makes this evident.

Note, however, that some decay in the mean magnetic energy is apparent after approximately $t = 15.7$ (see figure 10). At this time, the mean magnetic energy equals 0.75402, or 99.74 % of its initial value. This decay of the mean magnetic field indicates that the nonlinear terms have become significant. Hence the linear theory, which assumes the stationarity of the mean, does not by this time serve as an adequate

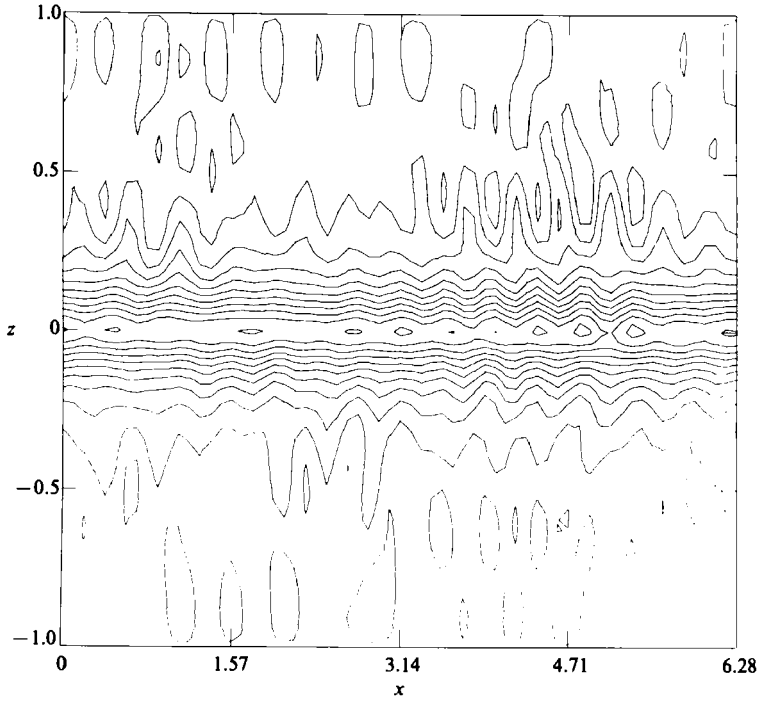

FIGURE 4. Run D; contour plot of electric current density at $t = 0$. The maximum contour value is 8.16. The minimum contour value is -0.765.

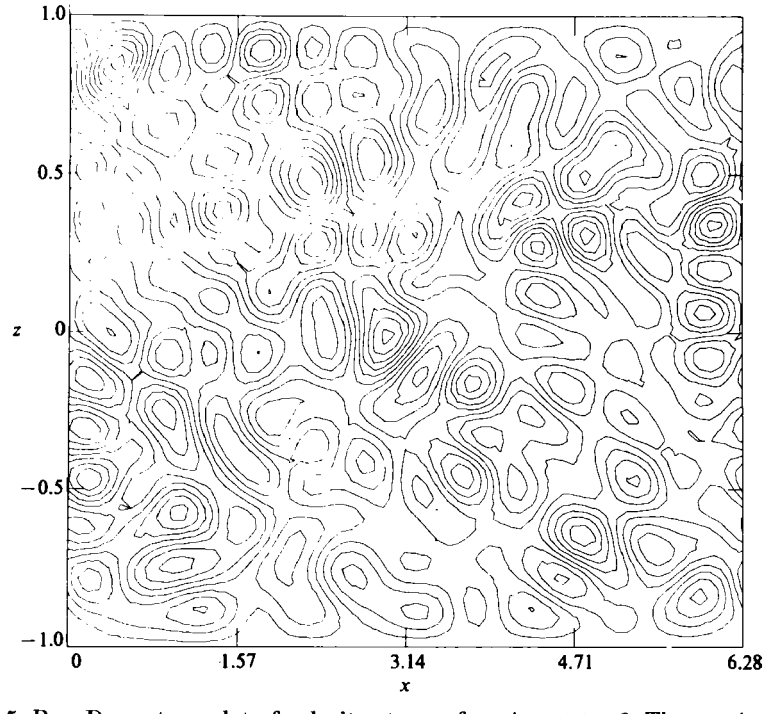

FIGURE 5. Run D; contour plot of velocity stream function at $t = 0$. The maximum contour value is 0.00436. The minimum contour value is -0.00451.

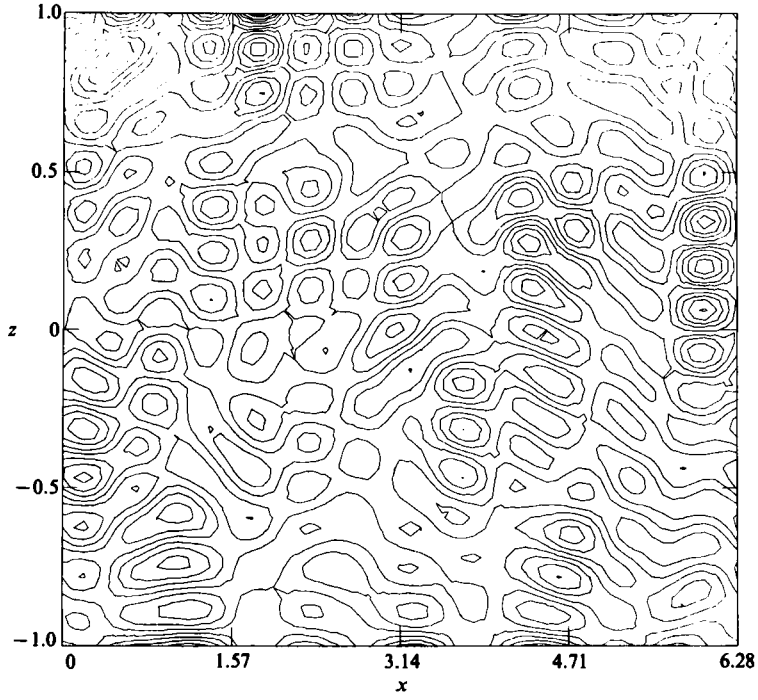

FIGURE 6. Run D; contour plot of vorticity at $t = 0$. The maximum contour value is 2.12. The minimum contour value is -1.61.

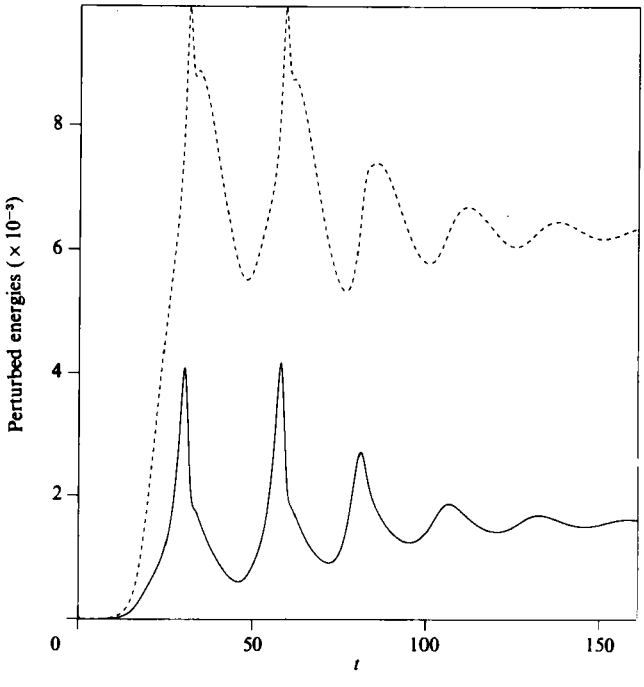

FIGURE 7. Run D; perturbed energies *vs.* time. Solid line, kinetic energy; dashed line, perturbed magnetic energy.

k_x	Growth rate
1	0.203
2	0.252
3	0.181

TABLE 3. Linear growth rates for $B_0(z) = \arctan(8z)$, $M = S = 200$.

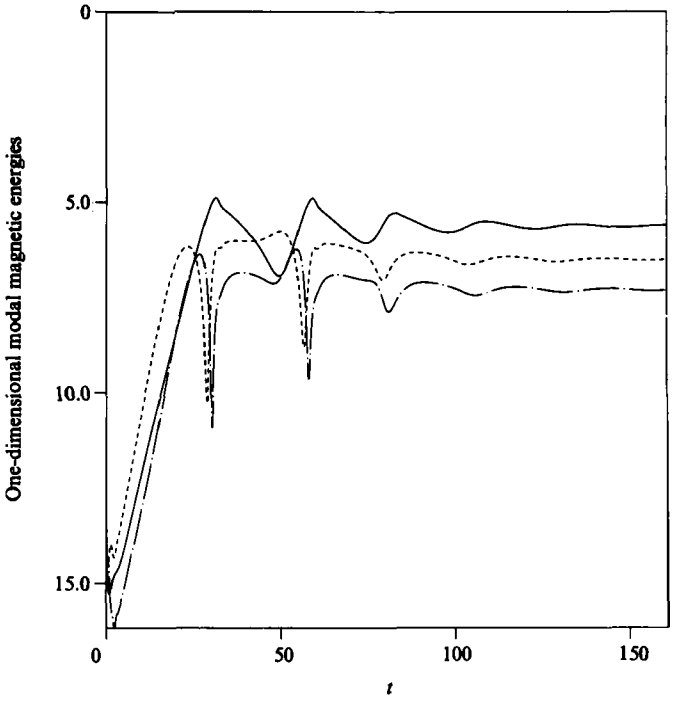

FIGURE 8. Run D; natural logarithm of one dimensional modal magnetic energies *vs.* time. Solid line, $k_x = 1$; dashed line, $k_x = 2$; mixed line, $k_x = 3$.

description of the behaviour of the system. The time at which the perturbations attain finite amplitude can be inferred from the ratios of the perturbed energies to the mean magnetic energy (see table 2). At $t = 15.708$, the perturbed magnetic energy is 0.059 % of the mean magnetic energy, and the kinetic energy is 0.022 % of the mean magnetic energy. This is not very different from the initial value of these ratios. What is different is that the perturbed energy is now more concentrated in the $k_x = 2$ and $k_x = 1$ modes than it was initially. The consequence of this concentration is the activation of the nonlinearities. Figures 11–14 are contour plots of the scalar fields at this time. Note especially the presence of the two magnetic X-points. The presence of two magnetic O-points is indicated by the bending of the contours of constant magnetic vector potential.

The two magnetic O-points soon merge. The system achieves its maximum nonlinearity at the conclusion of this coalescence process, which occurs at approximately $t = 31$. At $t = 31.416$, near to this time, the perturbed magnetic energy is 1.46 % of the mean magnetic energy, and the kinetic energy is 0.44 % of the mean

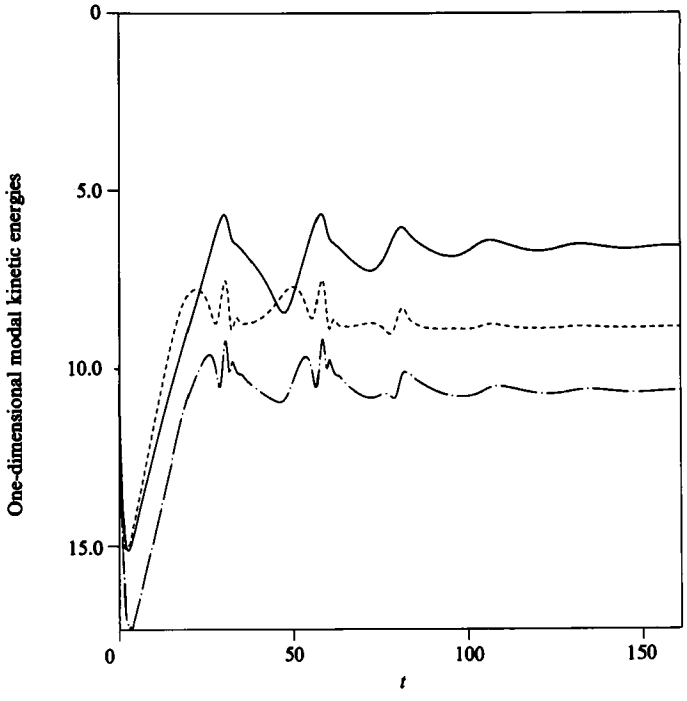

FIGURE 9. Run D; natural logarithm of one dimensional modal kinetic energies *vs.* time. Solid line, $k_x = 1$; dashed line, $k_x = 2$; mixed line, $k_x = 3$.

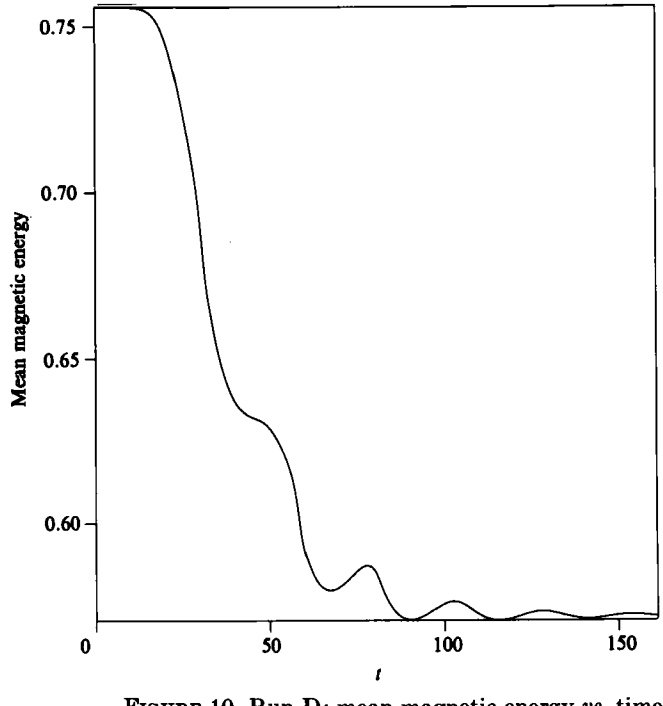

FIGURE 10. Run D; mean magnetic energy *vs.* time.

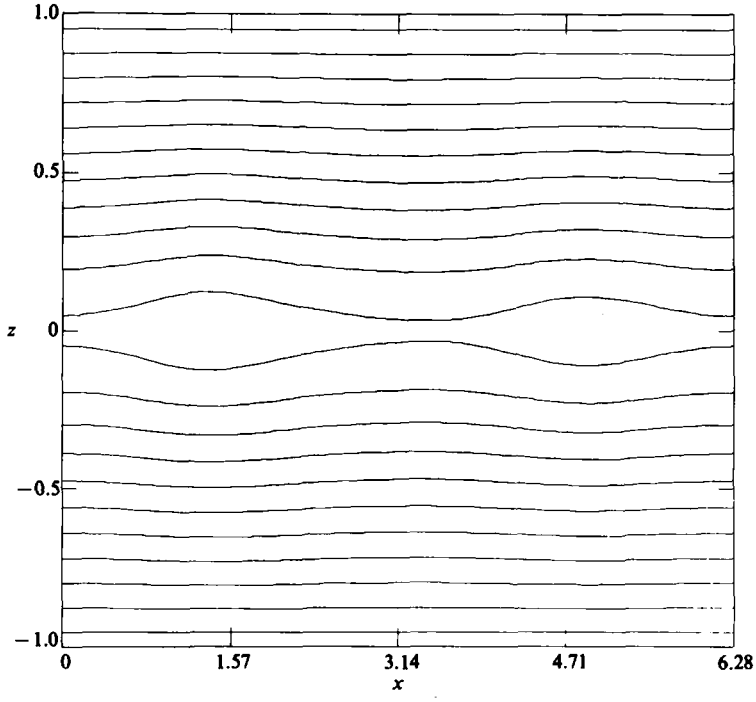

FIGURE 11. Run D; contour plot of magnetic vector potential at $t = 15.708$. The maximum contour value is 1.20. The minimum contour value is 0.100.

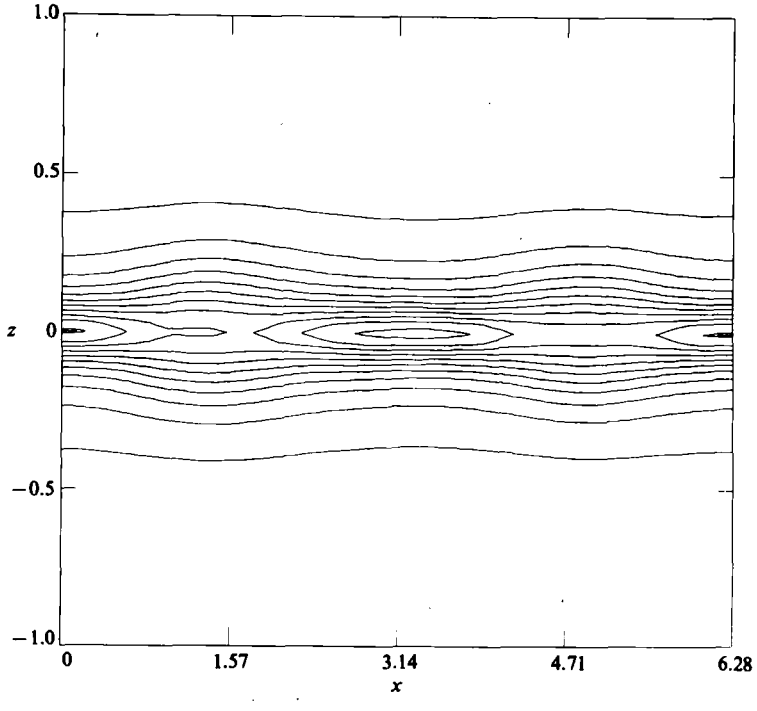

FIGURE 12. Run D; contour plot of electric current density at $t = 15.708$. The maximum contour value is 8.51. The minimum contour value is 0.709.

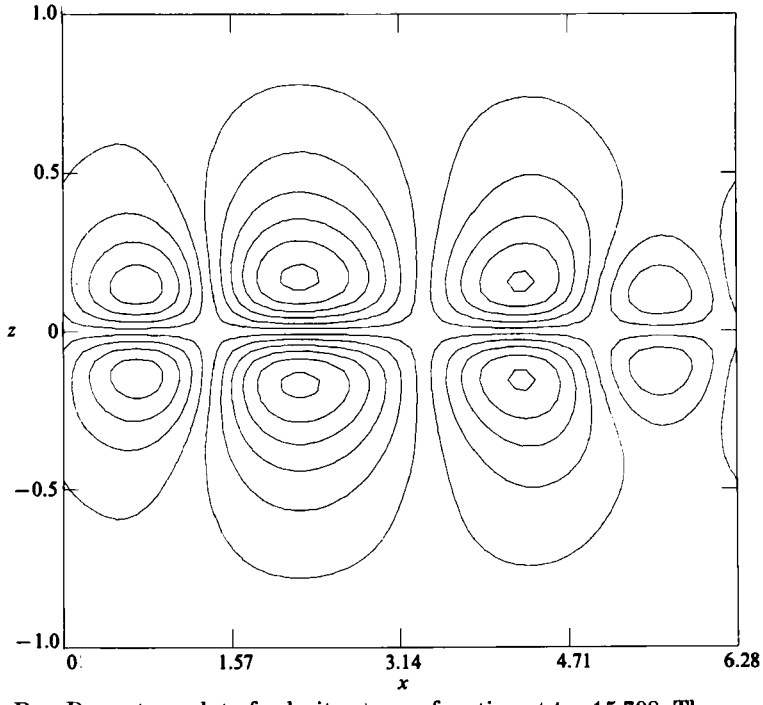

FIGURE 13. Run D; contour plot of velocity stream function at $t = 15.708$. The maximum contour value is 0.009 16. The minimum contour value is −0.009 14. The direction of flow into the magnetic X-point located near the centre of this plot is from the top and bottom.

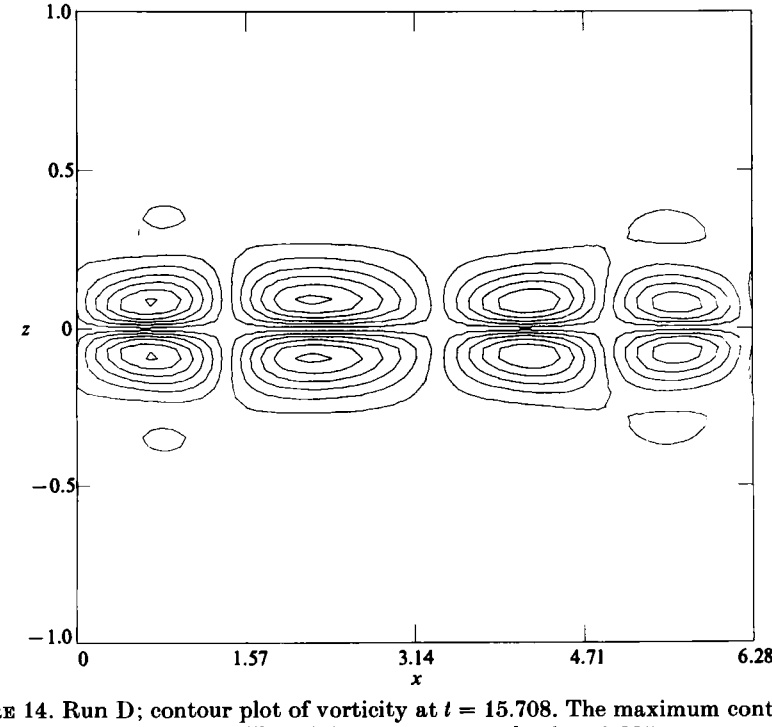

FIGURE 14. Run D; contour plot of vorticity at $t = 15.708$. The maximum contour value is 0.825. The minimum contour value is −0.825.

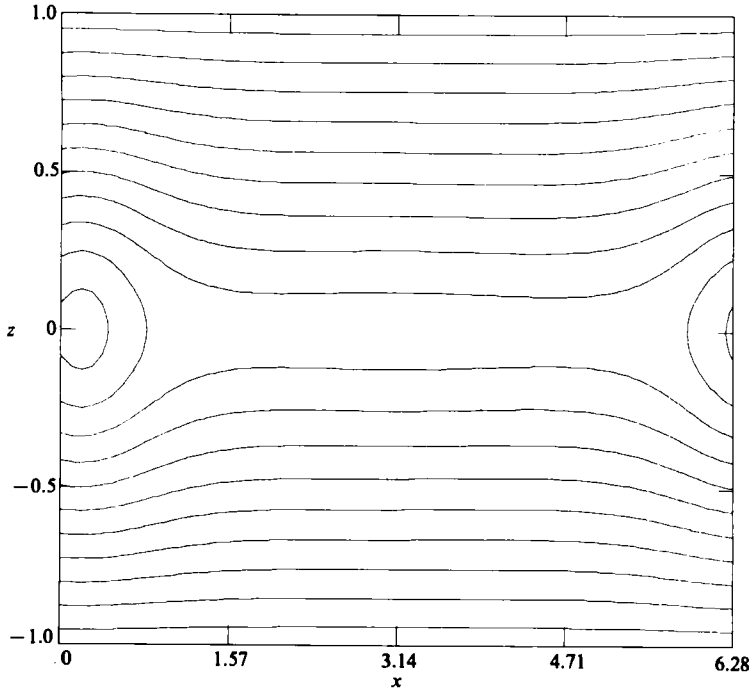

FIGURE 15. Run D; contour plot of magnetic vector potential at $t = 31.416$. The maximum contour value is 1.27. The minimum contour value is 0.106.

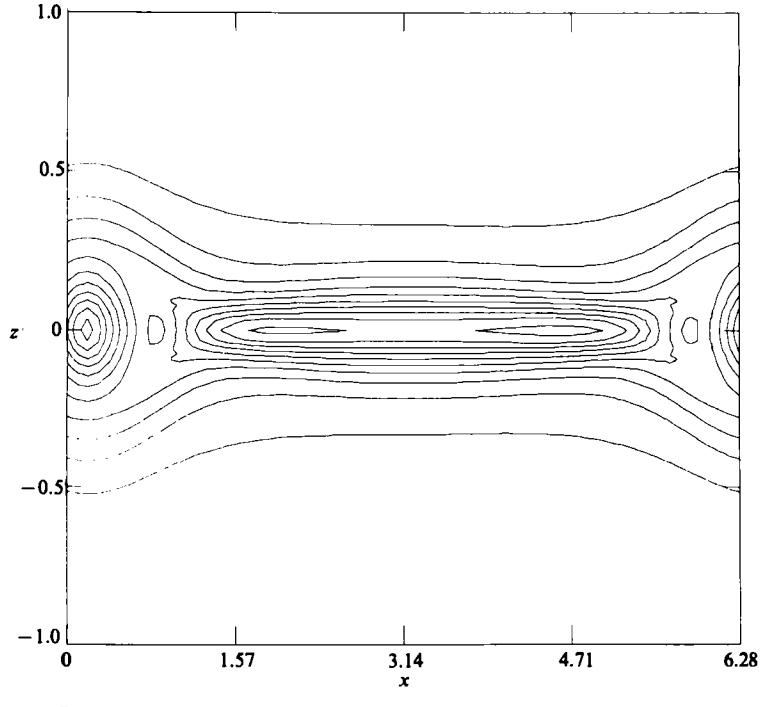

FIGURE 16. Run D; contour plot of electric current density at $t = 31.416$. The maximum contour value is 8.59. The minimum contour value is 0.716.

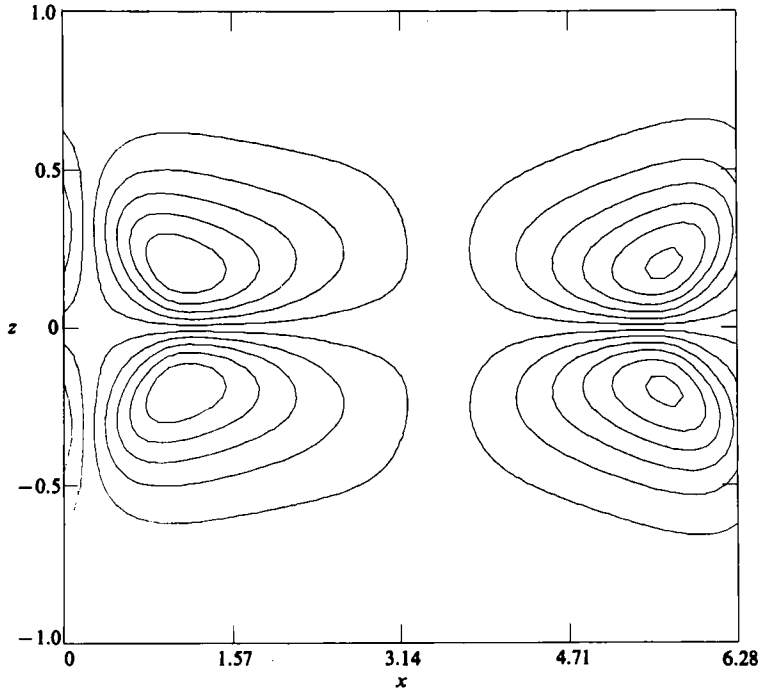

FIGURE 17. Run D; contour plot of velocity stream function at $t = 31.416$. The maximum contour value is 0.0244. The minimum contour value is -0.0244. The direction of flow into the magnetic X-point located near the centre of this plot is from the top and bottom.

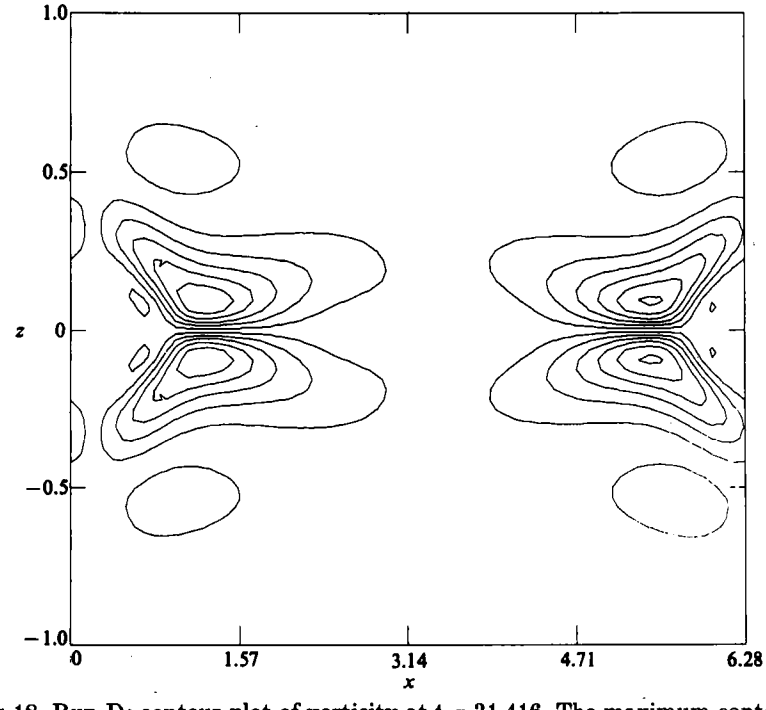

FIGURE 18. Run D; contour plot of vorticity at $t = 31.416$. The maximum contour value is 1.78. The minimum contour value is -1.78.

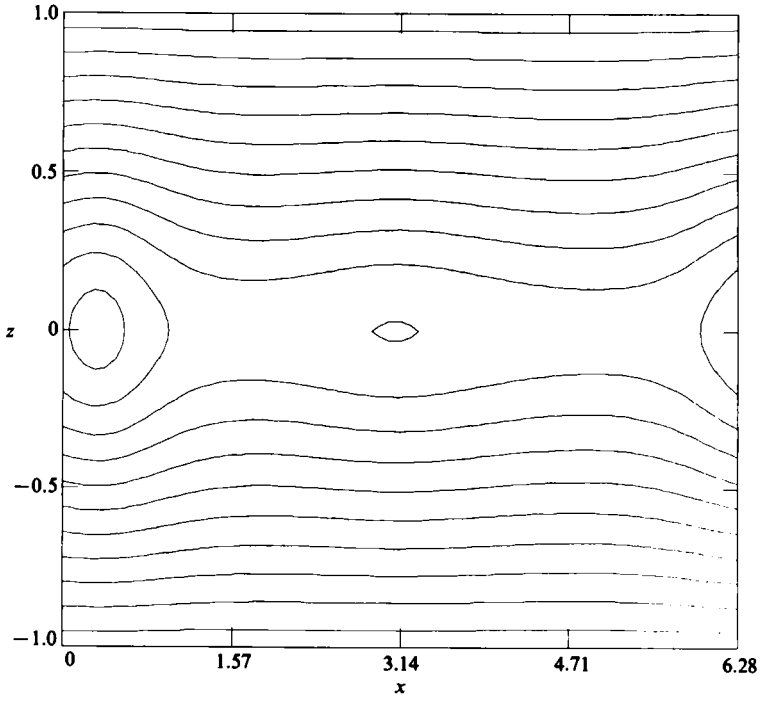

FIGURE 19. Run D; contour plot of magnetic vector potential at $t = 47.125$. The maximum contour value is 1.23. The minimum contour value is 0.103.

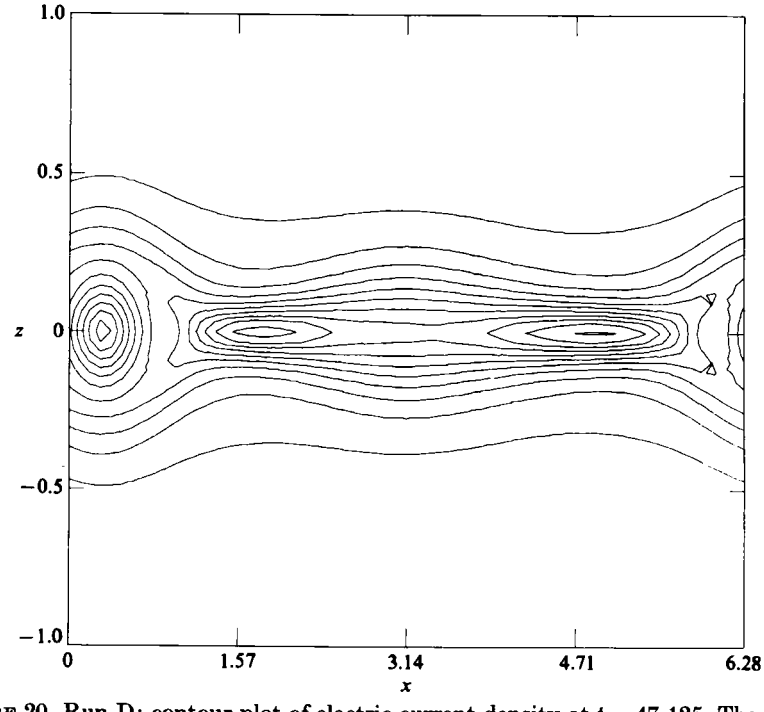

FIGURE 20. Run D; contour plot of electric current density at $t = 47.125$. The maximum contour value is 8.52. The minimum contour value is 0.710.

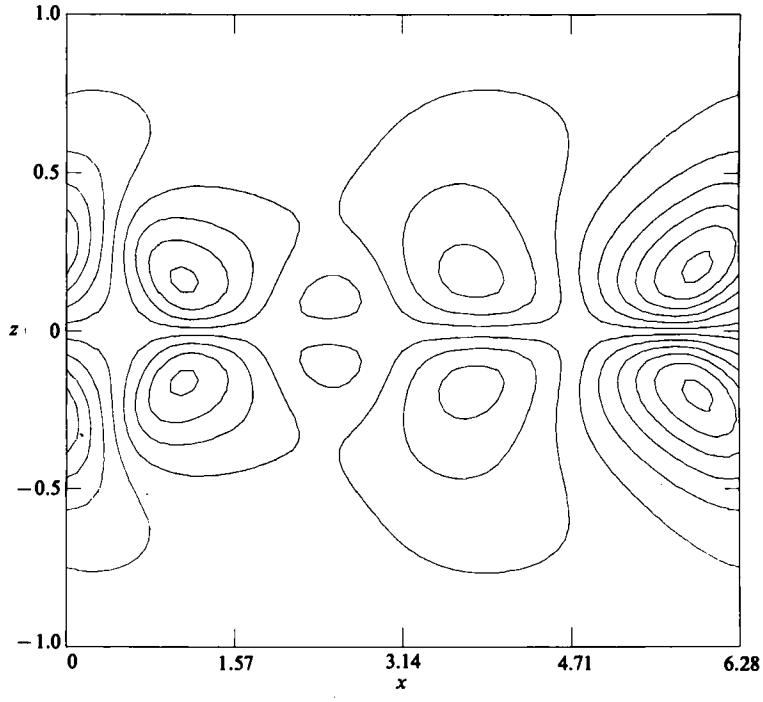

FIGURE 21. Run D; contour plot of velocity stream function at $t = 47.125$. The maximum contour value is 0.0220. The minimum contour value is -0.0220. The direction of flow out of the magnetic O-point located near ($x = 0$, $z = 0$) is towards the top and bottom.

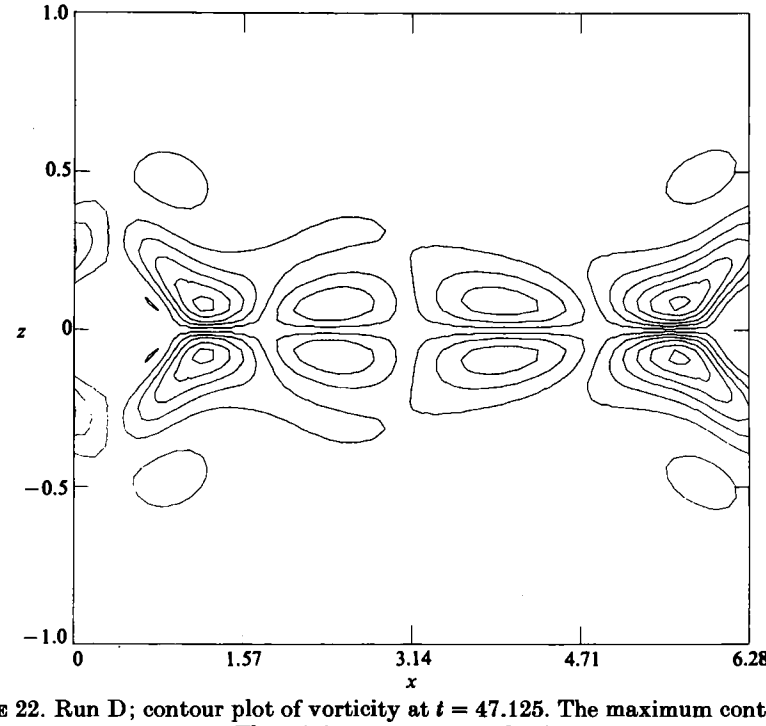

FIGURE 22. Run D; contour plot of vorticity at $t = 47.125$. The maximum contour value is 1.77. The minimum contour value is -1.77.

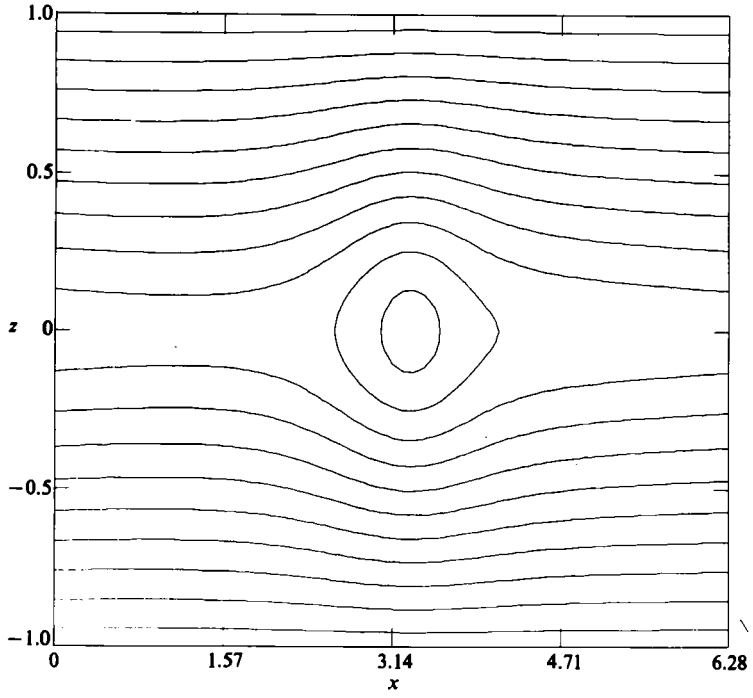

FIGURE 23. Run D; contour plot of magnetic vector potential at $t = 161.009$. The maximum contour value is 1.19. The minimum contour value is 0.099.

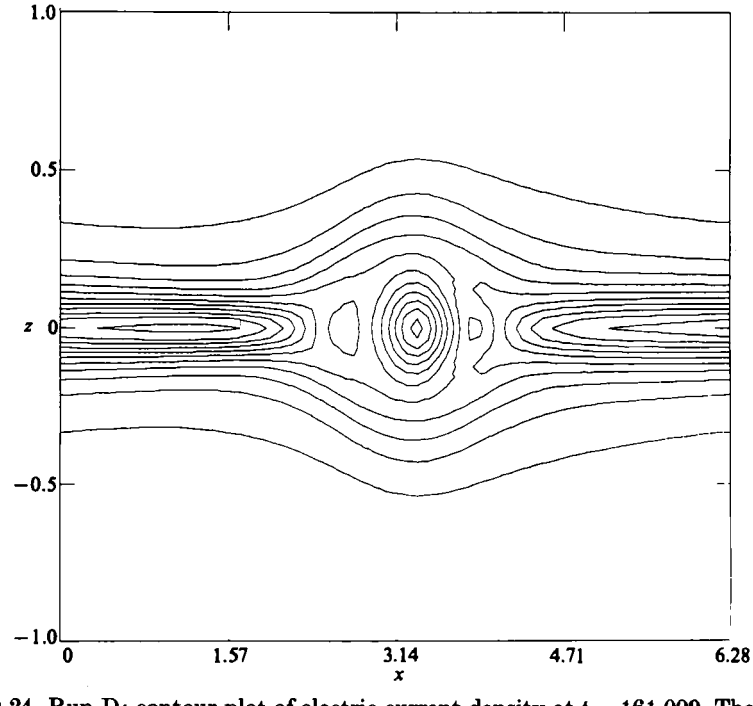

FIGURE 24. Run D; contour plot of electric current density at $t = 161.009$. The maximum contour value is 7.68. The minimum contour value is 0.640.

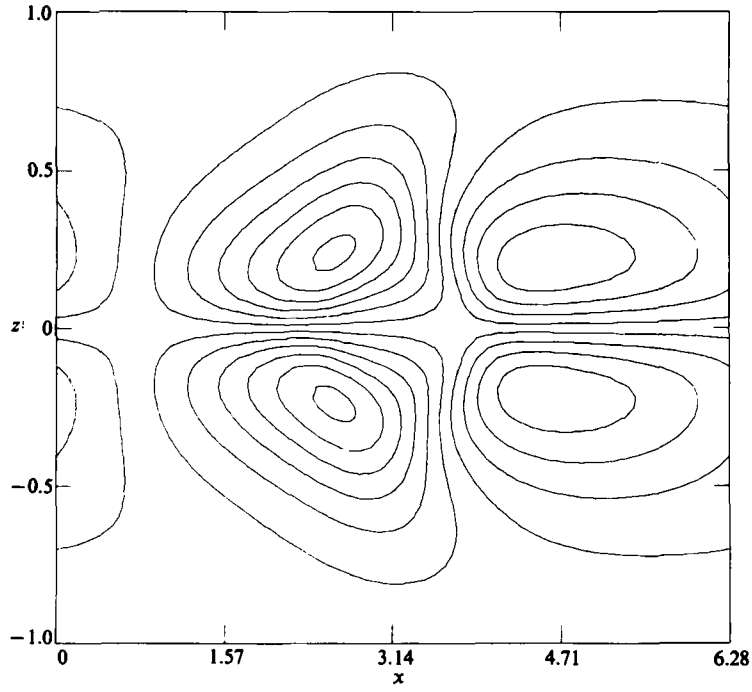

FIGURE 25. Run D; contour plot of velocity stream function at $t = 161.009$. The maximum contour value is 0.0318. The minimum contour value is −0.0319. The direction of flow out of the magnetic O-point located near the centre of this plot is towards the top and bottom.

magnetic energy (see table 2). Maximum nonlinearity is characterized by two structures which appear in the electric current. First, an electric current sheet of finite extent in the x direction is seen to form. Second, the electric current in the vicinity of the magnetic O-point increases in magnitude and becomes peaked. This latter field configuration gives rise to an approximately radially inward Lorentz force towards the magnetic O-point. Hence these electric currents can be termed 'attraction currents'. Figures 15 to 18 are contour plots of the scalar fields at $t = 31.416$, near the time of maximum nonlinearity.

Contour plots at a later time, $t = 47.125$, show that this configuration is itself subject to instabilities (figures 19–22). The electric current sheet splits into two filaments, around each of which forms the distinctive structure of eddies, magnetic O-points, etc. (Matthaeus & Montgomery 1981). This secondary instability is apparently of a different kind than those seen earlier in the run (cf. Syrovatskii 1979; Biskamp 1984). The earlier instabilities were those appropriate to the infinite plane current layer. In contrast, the electric current sheet is a nonlinear structure of finite extent in the x-direction. Furthermore, the infinite plane current layer is a static configuration, whereas the finite current sheet is essentially dynamic. From its inception, there is a significant flow of magnetofluid into and out of the current sheet.

This dynamic tearing of the electric current sheet implies the formation of multiple magnetic O-points. A second magnetic O-point is seen to form, and then begin coalescing with the original magnetic O-point. This phase of coalescence leads to the second peak in the perturbed energies. These processes repeat themselves, leading to

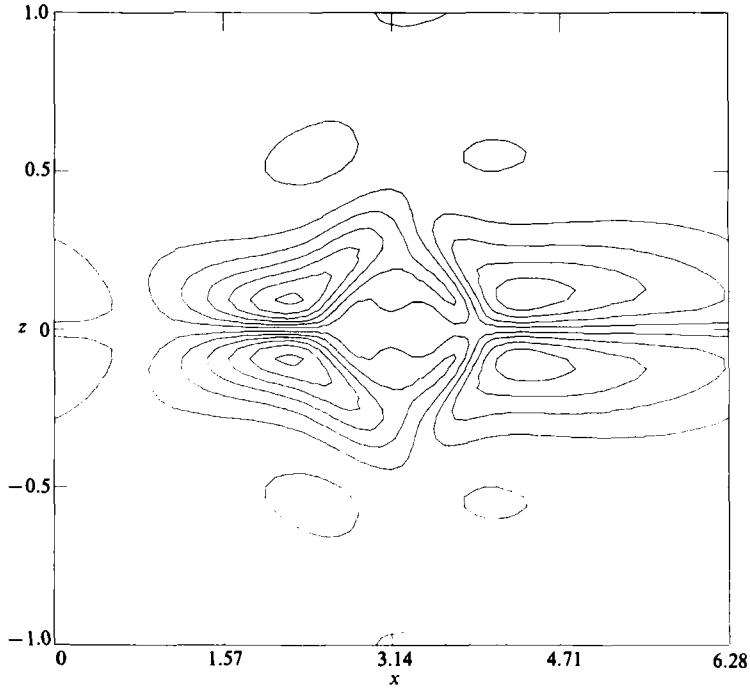

FIGURE 26. Run D; contour plot of vorticity at $t = 161.009$. The maximum contour value is 1.92. The minimum contour value is −1.92.

sawtooth-like temporal oscillations in the perturbed energies. Coincident with this, the mean magnetic energy is seen to approach a constant value (figure 10).

The ultimate state achieved resembles a state of secondary equilibrium, with many wavenumbers of the system being excited. At $t = 161.009$, the ultimate time achieved, the mean magnetic energy has decayed to approximately 75.6 % of its initial value (see table 2). Comparison of the initial and final mean magnetic vector potential is made in figure 1. The same comparison is made for the electric current density in figure 2. At this time the perturbed magnetic energy is 1.11 % of the mean magnetic energy. The kinetic energy is 0.28 % of the mean magnetic energy. Figures 23–26 are contour plots of the scalar fields at the ultimate time, $t = 161.009$. This field configuration has existed almost unchanged since approximately $t = 100$, although the magnetic 0-point has exhibited a slight drift in the positive x-direction. Note that the presence of regions of high vorticity implies that viscous dissipation is a non-ignorable process. This is borne out by a consideration of the systems' energetics at the final computed time, i.e. $t = 161.009$. The ohmic dissipation of the mean magnetic energy is given by:

$$2\pi \int_{-1}^{1} \eta(z) J_0^2(z, t = 161.009)\, \mathrm{d}z = 0.635\,15.$$

The ohmic disipation of the perturbed magnetic energy is given by:

$$\int_0^{2\pi} \int_{-1}^{1} \eta(z) j^2(x, z, t = 161.009)\, \mathrm{d}x\, \mathrm{d}z = 0.015\,828.$$

The viscous dissipation of the kinetic energy is given by:

$$\nu \int_0^{2\pi} \int_{-1}^{1} \omega^2(x, z, t = 161.009)\, dx\, dz = 0.011039.$$

Due to the amount of computer time required to perform these numerical simulations, it was impractical to perform an extensive investigation of the variation of the system's behaviour in response to changes in the parameters. However, some comparisons can be made between run D and certain of the other runs listed in table 1. In run C, which was performed at a lower value of the Lundquist numbers, the disturbance saturated at a much earlier time and at a larger magnitude. Furthermore, the decay of the mean magnetic field was somewhat less than in run D. Run E, which was performed at higher values of the Lundquist number than run D, was not continued to saturation because the numerical resolution was compromised. In this run the peak perturbed energies were somewhat larger than in run D, and when these peaks were attained the excitation of high wavenumbers was severe. The decay of the mean magnetic field in run E was similar to that in run D (Dahlburg 1985).

5. Nonlinear analysis

We present here an analysis which reproduces many of the features observed in the numerical simulations. This method was first employed, in a hydrodynamical context, by Stuart (1958) in a study of the nonlinear stability properties of plane Poiseuille flow and Taylor–Couette flow. The principal assumption underlying the analysis is that the generation of higher harmonics of the initial disturbance is insignificant, which implies that the most important nonlinear effect is the distortion of the mean field profile. Starting from the Reynolds–Orr energy equation, Stuart derived a Landau nonlinear stability equation (e.g. Landau & Lifschitz 1959) which described the nonlinear behaviour of linearly supercritical instabilities.

In order to simplify the problem of the nonlinear behaviour of the driven MHD sheet pinch, we consider the evolution of a single linearly unstable mode into the nonlinear regime. When this primary mode attains finite amplitude there are several consequences due to the activation of the nonlinear terms. The mode will interact with itself and so generate a secondary harmonic disturbance. The mode will interact with its complex conjugate and so act to deform the mean profile. Last, higher harmonics of the disturbance will be generated which can act to deform the original primary unstable mode.

Information about the nonlinear evolution of the disturbance can be obtained through consideration of the perturbation energy balance. We consider the following form of the fields:

$$\left.\begin{aligned} A(x, z, t) &= \overline{A}(z, t) + a'(x, z, t), \\ \psi(x, z, t) &= \phi'(x, z, t), \end{aligned}\right\} \tag{5.1}$$

where $\overline{A}(z, t)$ is defined to be the mean magnetic vector potential. The primed quantities represent periodic disturbances with no mean part and of arbitrary magnitude. If these primed fields are of finite amplitude, then the mean magnetic vector potential will be deformed, so that its time dependence must be taken into

account. Using these fields and the governing equations (2.1), a perturbation energy balance can be derived:

$$\begin{aligned}\frac{1}{2}\frac{\partial}{\partial t}\int_0^{2\pi}\int_{-1}^{1}\left[\left(\frac{\partial\phi'}{\partial z}\right)^2+\left(\frac{\partial\phi'}{\partial x}\right)^2+\left(\frac{\partial a'}{\partial z}\right)^2+\left(\frac{\partial a'}{\partial x}\right)^2\right]\mathrm{d}x\,\mathrm{d}z\\ =\int_0^{2\pi}\int_{-1}^{1}\left(\frac{\partial\phi'}{\partial z}\frac{\partial a'}{\partial x}-\frac{\partial\phi'}{\partial x}\frac{\partial a'}{\partial z}\right)\frac{\partial^2\overline{A}}{\partial z^2}\mathrm{d}x\,\mathrm{d}z\\ -\frac{1}{S}\int_0^{2\pi}\int_{-1}^{1}\xi(z)\left(\frac{\partial^2 a'}{\partial x^2}+\frac{\partial^2 a'}{\partial z^2}\right)^2\mathrm{d}x\,\mathrm{d}z\\ -\frac{1}{M}\int_0^{2\pi}\int_{-1}^{1}\left(\frac{\partial^2\phi'}{\partial x^2}+\frac{\partial^2\phi'}{\partial z^2}\right)^2\mathrm{d}x\,\mathrm{d}z,\end{aligned}\tag{5.2}$$

where $\xi(z)=S\eta(z)$.

Equation (5.2) is the driven magnetohydrodynamic equivalent of the Reynolds–Orr energy equation for neutral fluids. The term on the left-hand side of (5.2) is the rate of change of the total perturbed energy, i.e. both magnetic and kinetic. The first integral on the right-hand side of (5.2) represents the interchange of energy between the mean magnetic field and the perturbed fields. The direction of the energy exchange depends on the sign of this interchange integral. If it is positive it represents a transfer of energy from the mean magnetic field to the perturbed fields. If it is negative it represents a transfer of energy from the perturbed fields to the mean field. The second integral term on the right-hand side represents the perturbed magnetic energy losses due to ohmic dissipation. The third integral term represents the kinetic energy losses due to viscous dissipation. These two dissipative integrals are always positive. Note that growth of the perturbations is possible only if the interchange integral is positive and of a magnitude which exceeds the sum of the two dissipative integrals. Furthermore, note that the perturbation energy balance implies that a state of equilibrium occurs when the interchange integral is equal to the sum of the dissipative integrals.

It it assumed that the only significant nonlinear interactions occur among the mean magnetic vector potential and the primary disturbance (magnetic and velocity), which implies that the generation of higher harmonics of the primary disturbance is a negligible process. This further implies that the distortion of the primary disturbance will be negligible.

On the basis of these assumptions, we consider the effect of the finite amplitude perturbation on the mean magnetic vector potential. The equation for the magnetic vector potential is, in the (A,ψ) form:

$$\frac{\partial A}{\partial t}-\frac{\xi(z)}{S}\left(\frac{\partial^2 A}{\partial x^2}+\frac{\partial^2 A}{\partial z^2}\right)-E=\frac{\partial\psi}{\partial z}\frac{\partial A}{\partial x}-\frac{\partial\psi}{\partial x}\frac{\partial A}{\partial z},\tag{5.3}$$

where the nonlinear terms have been isolated on the right-hand side. In accord with the assumptions, A and ψ can be expanded as follows:

$$\left.\begin{aligned}A(x,z,t)&=A_0(z,t)+\hat{a}(z,t)\,\mathrm{e}^{\mathrm{i}\alpha x}+\hat{a}^*(z,t)\,\mathrm{e}^{-\mathrm{i}\alpha x},\\ \psi(x,z,t)&=\hat{\phi}(z,t)\,\mathrm{e}^{\mathrm{i}\alpha x}+\hat{\phi}^*(z,t)\,\mathrm{e}^{-\mathrm{i}\alpha x},\end{aligned}\right\}\tag{5.4}$$

where * denotes the complex-conjugate, and α is defined to be the wavenumber of the disturbance parallel to the magnetic field.

Upon substitution, the mean magnetic vector potential equation is found to be:

$$\frac{\partial A_0}{\partial t}-\frac{\xi(z)}{S}\frac{\partial^2 A_0}{\partial z^2}-E=\mathrm{i}\alpha\frac{\partial}{\partial z}(\hat{\alpha}\hat{\phi}^*-\hat{\alpha}^*\hat{\phi}). \tag{5.5}$$

When $\partial A_0/\partial t$ is negligible, (5.5) will give an expression for the nonlinearly saturated mean electric current density.

We now employ the 'shape assumption' (Stuart 1958), i.e. we assume that the primary disturbance is equal to the unstable eigenmode of the system multiplied by a time amplification factor $\lambda(t)$:

$$\left.\begin{aligned} A(x,z,t) &= A_0(z,t)+\lambda(t)\,[a(z)\,\mathrm{e}^{\mathrm{i}\alpha x}+a^*(z)\,\mathrm{e}^{-\mathrm{i}\alpha x}],\\ \psi(x,z,t) &= \lambda(t)\,[\phi(z)\,\mathrm{e}^{\mathrm{i}\alpha x}+\phi^*(z)\,\mathrm{e}^{\mathrm{i}\alpha x}], \end{aligned}\right\} \tag{5.6}$$

where $a(z)$ = magnetic eigenfunction, $\phi(z)$ = velocity eigenfunction.

The eigenfunctions are solutions of the equations for the linear instabilities of the system. By means of a normal mode analysis (e.g. Dahlburg *et al.* 1983), these equations are found to take the following form:

$$\left.\begin{aligned} &(\mathrm{D}^2-\alpha^2)^2\phi=-\mathrm{i}\omega M(\mathrm{D}^2-\alpha^2)\phi+\mathrm{i}\alpha M(\mathrm{D}A_0)(\mathrm{D}^2-\alpha^2)a-\mathrm{i}\alpha M(\mathrm{D}^3A_0)a,\\ &\{\mathrm{D}^2-\alpha^2+\mathrm{i}\omega S\zeta(z)\}a=\mathrm{i}\alpha S\zeta(z)(\mathrm{D}A_0)\phi,\\ &\phi(z=1)=\phi(z=-1)=0,\quad a(z=1)=a(z=-1)=0, \end{aligned}\right\} \tag{5.7}$$

where $\mathrm{D}=\mathrm{d}/\mathrm{d}z$, ω = complex eigenfrequency, $\zeta(z)=1/\xi(z)$ = dimensionless conductivity.

These equations are solved numerically by a modification of the algorithm described by Dahlburg *et al.* (1983). This algorithm is based on the Chebyshev-tau method devised by Orszag (1971) for numerical solution of the Orr–Sommerfeld equation. It is found that for the unstable modes, the perturbed magnetic vector potential is always real, whereas the perturbed stream function is always imaginary. Furthermore, the unstable modes have zero phase velocity. This implies that on the neutral stability surface the complex eigenfrequency is equal to zero. It can be shown that in this case the locus of critical points in the (M,S)-space takes the form of a hyperbola, with α equal to a constant value (Dahlburg *et al.* 1983; Dahlburg 1985).

With the shape assumption, the mean field equation becomes

$$\frac{\partial A_0}{\partial t}-\frac{\xi(z)}{S}\frac{\partial^2 A_0}{\partial z^2}-E=2\alpha\lambda^2\frac{\mathrm{d}}{\mathrm{d}z}(a_\mathrm{r}\phi_\mathrm{i}), \tag{5.8}$$

where the subscripts r and i respectively denote the real and imaginary part of the eigenfunction.

In the vicinity of the locus of critical points, $\partial A_0/\partial t$ is negligible, and the mean field equation reduces to:

$$-\frac{\mathrm{d}^2A_0}{\mathrm{d}z^2}=J_0(z)=S\zeta(z)\,E+2\alpha\lambda^2 S(z)\frac{\mathrm{d}}{\mathrm{d}z}(a_\mathrm{r}\phi_\mathrm{i}). \tag{5.9}$$

In the vicinity of the neutral curve, this last expression can be used in the perturbation energy balance, which by the shape assumption takes the form

$$\gamma_1\frac{\mathrm{d}\lambda^2}{\mathrm{d}t}=-4\alpha^2S\gamma_2\lambda^4-2\left(\alpha SE\gamma_3+\frac{1}{M}\gamma_4+\frac{1}{S}\gamma_5\right)\lambda^2, \tag{5.10}$$

where

$$\left.\begin{aligned}
\gamma_1 &\equiv \int_{-1}^{1}\left[\left(\frac{\mathrm{d}\phi_\mathrm{i}}{\mathrm{d}z}\right)^2+\alpha^2\phi_\mathrm{i}^2+\left(\frac{\mathrm{d}a_\mathrm{r}}{\mathrm{d}z}\right)^2+\alpha^2 a_\mathrm{r}^2\right]\mathrm{d}z,\\
\gamma_2 &\equiv \int_{-1}^{1}\zeta(z)\left[\frac{\mathrm{d}}{\mathrm{d}z}(a_\mathrm{r}\phi_\mathrm{i})\right]^2\mathrm{d}z,\\
\gamma_3 &\equiv \int_{-1}^{1}\zeta(z)\left[\frac{\mathrm{d}}{\mathrm{d}z}(a_\mathrm{r}\phi_\mathrm{i})\right]\mathrm{d}z,\\
\gamma_4 &\equiv \int_{-1}^{1}\left[\left(\frac{\mathrm{d}^2\phi_\mathrm{i}}{\mathrm{d}z^2}\right)^2+2\alpha^2\left(\frac{\mathrm{d}\phi_\mathrm{i}}{\mathrm{d}z}\right)^2+\alpha^4\phi_\mathrm{i}^2\right]\mathrm{d}z,\\
\gamma_5 &\equiv \int_{-1}^{1}\left\{\xi(z)\left[\left(\frac{\mathrm{d}^2 a_\mathrm{r}}{\mathrm{d}z^2}\right)^2+\alpha^4 a_\mathrm{r}^2\right]+\alpha^2\left[2\xi(z)\left(\frac{\mathrm{d}a_\mathrm{r}}{\mathrm{d}z}\right)^2-\frac{\mathrm{d}^2\xi}{\mathrm{d}z^2}a_\mathrm{r}^2\right]\right\}\mathrm{d}z.
\end{aligned}\right\} \tag{5.11}$$

If we define

$$\left.\begin{aligned}
p(t) &\equiv \lambda^2(t),\\
C_1 &\equiv -\frac{2}{\gamma_1}\left(\alpha S E\gamma_3+\frac{1}{M}\gamma_4+\frac{1}{S}\gamma_5\right),\\
C_2 &\equiv \frac{4\alpha^2 S\gamma_2}{\gamma_1},
\end{aligned}\right\} \tag{5.12}$$

then the perturbation energy balance can be further reduced to

$$\frac{\mathrm{d}p}{\mathrm{d}t} = C_1 p - C_2 p^2. \tag{5.13}$$

This equation, first proposed by Landau (cf. Landau & Lifshitz 1959), is widely regarded as representing the essence of certain classes of weakly nonlinear behaviour (Herbert 1983). C_1 is the linear growth rate of the perturbed energies. C_2, which determines the strength of the nonlinear term, is often called the Landau constant. If the disturbance saturates nonlinearly, the saturated amplitude p_e is given by:

$$p_\mathrm{e} = \frac{C_1}{C_2}. \tag{5.14}$$

The integrals (equations (5.11)) can be numerically solved easily and accurately by Simpson's method. Certain of the results are compared with the benchmark results of the eigenvalue code to judge the accuracy of the expansion, where ω_i is defined to be the linear growth rate of the perturbation as computed by the eigenvalue code. Results are tabulated for $B_0(z) = \arctan(\gamma z)$ in table 4, where NC is defined to be the number of Chebyshev polynomials used in solving the eigenvalue problem (5.7).

We consider case 3 of table 4. The comparison seems likely to be closest in situations for which: (i) the extent $S-S_\mathrm{crit}$, by which S exceeds its linear stability threshold value S_crit, is small; and (ii) the initialization is in terms of a single eigenmode. For case 3 the locus of critical points in the (M, S)-plane is defined by $MS = 1074$, with α equal to 1.4. The amplitude phase plane for case 3 is shown in figure 27. For small p a region of exponential growth is seen. As p increases, the growth rate slows to less than exponential. At the equilibrium value, p_e, the growth rate is seen to equal zero. A prediction can be made for the form of the saturated mean electric current profile based on the mean magnetic vector potential equation (5.9). This prediction is shown in figure 28.

Case	γ	α	M	S	NC	ω_i	$\frac{1}{2}C_1$	C_2	p_e
1	8	1	50	50	66	0.090282	0.090278	1314	0.1374×10^{-3}
2	8	1	100	100	66	0.18223	0.18183	4372	0.8318×10^{-4}
3	8	2	100	100	60	0.22263	0.22257	60756	0.7327×10^{-5}
4	3	1	100	100	60	0.013658	0.013657	14156	0.3860×10^{-5}

TABLE 4. Results of nonlinear analysis. $B_0(z) = \arctan(\gamma z)$.

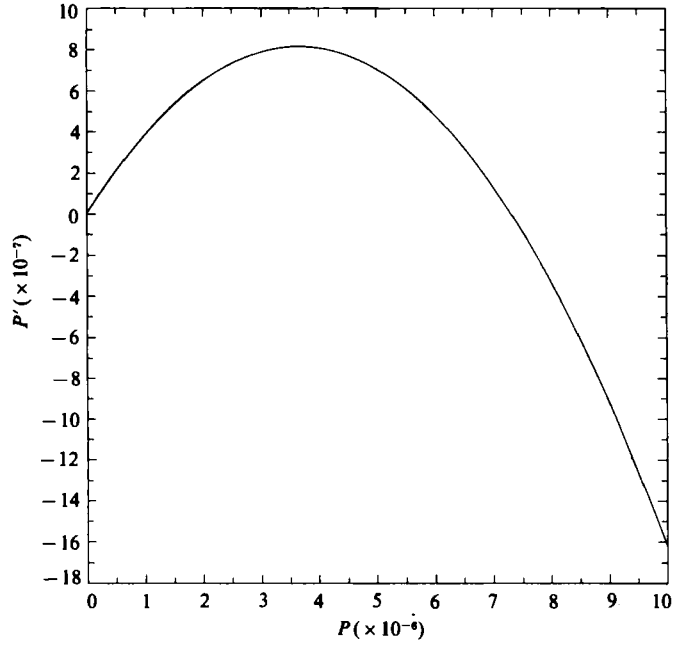

FIGURE 27. Amplitude phase plane for case 3.

The predictions can be compared with the results of run G (see table 1). The nonlinear code is initialized with the appropriate eigenmode, which is supplied by the linear code. The initial perturbations are shown in figure 29, where the z component of velocity is directly proportional to the perturbed stream function. The magnetic energy of the $k_x = 2$ mode and its first harmonic are exhibited as functions of time in figure 30. The one-dimensional modal kinetic energies are exhibited as functions of time in figure 31. The $k_x = 2$ magnetic and velocity modes are seen to grow linearly for about four e-folding times. As can be expected in solving the full nonlinear problem, the first harmonic of the primary disturbance is quickly generated, but its effect on the linear evolution of the system is negligible. It is seen that the $k_x = 2$ mode ceases growth at approximately $t = 20$, with cessation in the $k_x = 2$ kinetic energy slightly preceding the cessation in the $k_x = 2$ magnetic energy. At the ultimate time computed the perturbations have saturated. At this time the perturbed magnetic energy is 0.83 % of the mean magnetic energy, and the kinetic energy is 0.19 % of the mean magnetic energy. 82 % of the perturbed magnetic energy resides in the $k_x = 2$ mode, and 17 % in the $k_x = 4$ mode. 98 % of the kinetic energy resides in the $k_x = 2$ mode, and 1.9 % in the $k_x = 4$ mode. The assumption that the generation

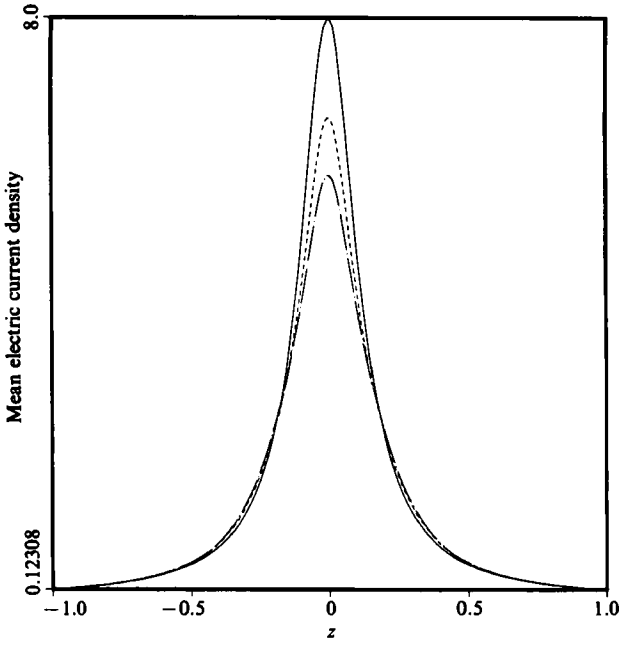

FIGURE 28. Case 3: mean electric current density profiles. Solid line, initial value; dashed line, computed saturated value (run G); mixed line, predicted saturated value.

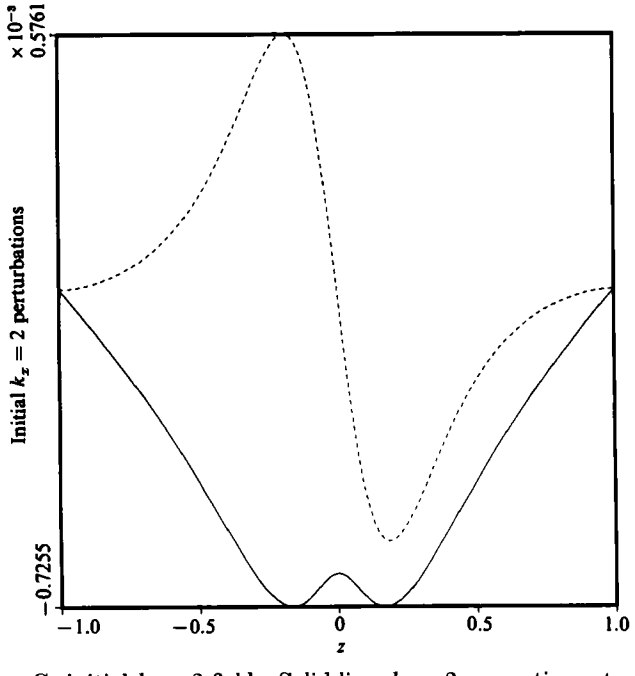

FIGURE 29. Run G; initial $k_z = 2$ fields. Solid line, $k_z = 2$ magnetic vector potential; dashed line, $k_z = 2$ z velocity component.

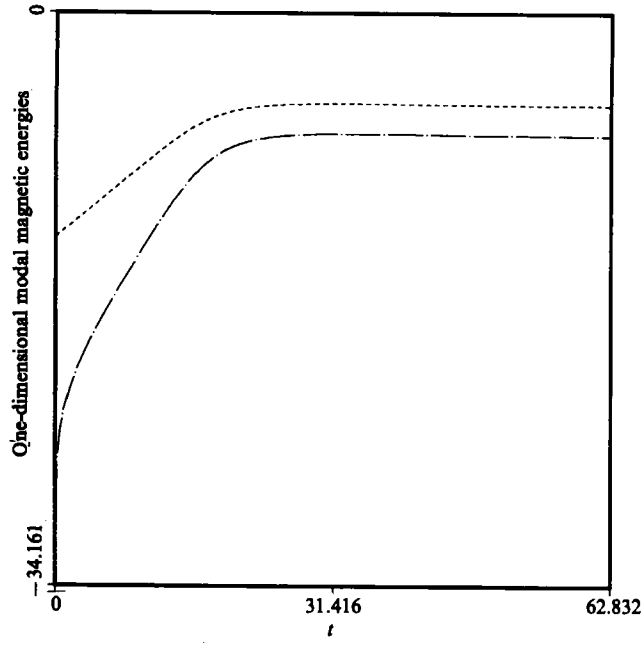

FIGURE 30. Run G; natural logarithm of one-dimensional modal magnetic energies *vs.* time. Dashed line, $k_x = 2$; mixed line, $k_x = 4$.

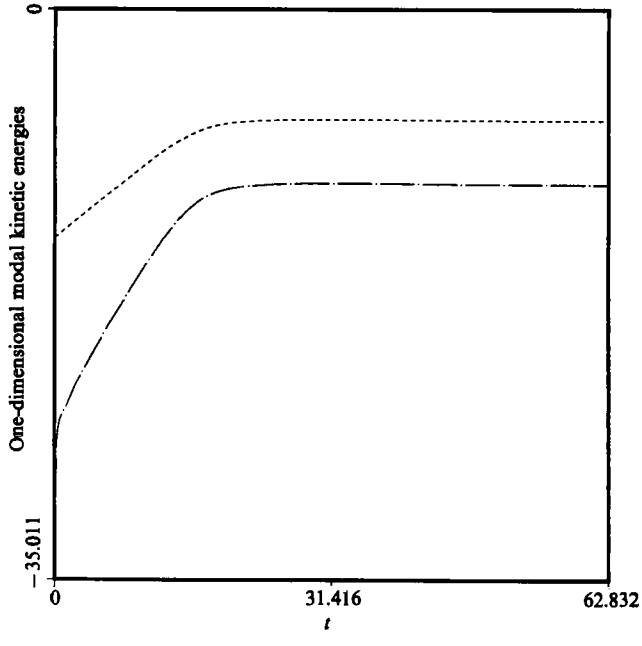

FIGURE 31. Run G; natural logarithm of one-dimensional modal kinetic energies *vs.* time. Dashed line, $k_x = 2$; mixed line, $k_x = 4$.

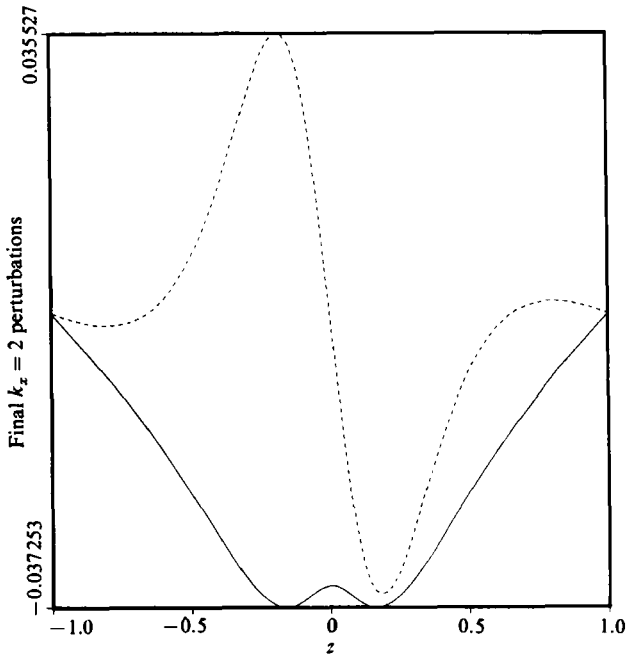

FIGURE 32. Run G; final $k_x = 2$ fields. Solid line, $k_x = 2$ magnetic vector potential; dashed line, $k_x = 2$ z velocity component.

of higher harmonics of the primary disturbance is negligible seems to be valid for the velocity modes, but not valid for the magnetic modes.

The form of the $k_x = 2$ magnetic and velocity modes at the ultimate time computed is shown in figure 32. The shape assumption appears to hold especially well for the magnetic disturbance. Some distortion is apparent in the velocity mode in the vicinity of the walls, and this distortion can be attributed to the presence of the higher harmonics.

The final mean electric current profile for run G is shown in figure 28. The peak value of the mean electric current density, as predicted by (5.9), is 5.86. The saturated value computed in run G is 6.63, so that the prediction of the peak value is in error by 11.6%.

The Stuart–Landau approach is based on the shape assumption and the neglect of the generation of higher harmonics. The shape assumption appears to be validated by the computations, whereas the neglect of the generation of higher harmonics of the primary disturbance does not. This is especially true of the magnetic disturbance. The saturated mean electric current density profile is not badly predicted by the Stuart–Landau approach, but this prediction could probably be improved by taking the higher harmonics of the disturbance into account.

6. Discussion

Determining the behaviour of the magnetohydrodynamic sheet pinch is an inherently difficult problem for two significant reasons. First, there is a lack of experimental data. This lack can be attributed to the difficulty of attaining data in the physical situations in which MHD sheet pinches occur. Second, due to the

complexity of the governing equations severe approximations are required to make any analytical headway. For these reasons much of the progress in understanding the fully nonlinear behaviour of the MHD sheet pinch has been made by means of numerical simulations.

Most previous numerical work has dealt with the pure decay case, whereas the present work has focused on the driven case, in which an external electric field and a spatially varying resistivity profile maintain the mean magnetic field against resistive decay. Without this driving, the mean magnetic field will decay ohmically in time even in the absence of perturbations. For the Lundquist numbers that are computationally accessible at present, this decay can be significant. With the driving we have employed, the decay of the mean magnetic field can only be initiated by nonlinear processes. Any alteration of the mean magnetic field will affect the energy transfer between the mean magnetic field and the perturbed fields. In the non-driven case, this energy transfer is variable from the outset due to the ohmic decay of the mean magnetic field. In the driven case, the energy transfer is altered only when the perturbations attain finite amplitude.

Possibly for this reason, the driven case exhibits phenomena which are not found in the decay case. First, from random initial perturbations multiple magnetic O-points are seen to arise (Matthaeus & Lamkin (1985) report a related result for the decay case initialized with large amplitude random perturbations). Secondly, different complex and highly nonlinear structures are seen to evolve in the electric current density, namely electric current sheets and attraction currents. Thirdly, a secondary instability, the dynamic tearing of the electric current sheet, is seen to occur. This leads to a spontaneous generation of multiple magnetic X-points, a feature not reported for the decay case. This dynamic tearing recurs, leading to sawtooth-like oscillations in some of the perturbed global quantities as functions of time.

The long time state of the driven system has also been investigated, both computationally and analytically. It is seen in the computations that a state resembling nonlinear saturation of the initial perturbations is achieved. The mean magnetic energy asymptotically approaches a constant value in time, while the perturbed energies remain at fairly constant values for many Alfvén transit times. The perturbed fields, which are defined as having no mean part, are composed of many excited x and z wavenumbers in the long time state.

The detailed structure which develops at long times has not been predicted analytically. It is characterized by the simultaneous presence of electric current filaments at the magnetic X-points, and attraction currents at the magnetic O-points. The peak value of the mean electric current decays from its initial value, and then remains approximately constant. Magnetofluid jets from the weak field corners of the magnetic X-point at a steady rate. Regions of high vorticity are seen in the vicinity of these jets. The presence of these regions of high vorticity implies that viscous dissipation is a non-ignorable process in the dynamics of the secondary equilibrium of the driven magnetohydrodynamic sheet pinch.

One noteworthy feature that has emerged from these computations is that the final-state quasi-equilibrium is not dominated by the linearly most unstable mode for the cases initialized with random noise (runs C and D), whereas this mode does ultimately dominate in the cases initialized with single eigenmodes (runs B and G). The final state of runs B and G was dominated by the $k_x = 2$ magnetic and velocity modes, which were linearly most unstable, although a significant fraction of the energy resided in the first harmonic of this disturbance. For the parameter ranges of runs C and D the most unstable linear mode was the $k_x = 2$ mode, but in the final

state of the computations many magnetic and velocity modes were excited, with the $k_x = 1$ modes being the largest.

The linear theory does describe quite well the initial phase of development in all of the runs performed. In the eigenmode initialized cases, harmonics are generated as would be expected in the fully nonlinear problem, but their effect on the initial growth of the primary disturbance is negligible. The random initialization runs exhibit an initial decay phase followed by exponential growth. This decay phase is perhaps due to the decay of the linearly damped modes, although this has not been verified.

No explanation has as yet emerged for the varied final state behaviour, but it is clear that it is in some way connected with the initial conditions. The eigenmode initialization will restrict the time evolution of the system to a smaller region of the available phase space than the random initialization will. This implies that more complex interactions among the wavenumbers are possible in the random initialization case, and that the nonlinear transfer of energy among the wavenumbers will be more varied than in the eigenmode initialized case.

It is perhaps significant that the walls do not enter strongly into the dynamics of the system. Some vorticity is seen to be convected from the walls into the region of the magnetic X-point, but it does not appear to significantly alter the magnetic reconnection process.

We are indebted to Dr M. Y. Hussaini for valuable discussions in the early stages of this research, and for making available some hydrodynamic shear-flow codes for modification. We would also like to thank an anonymous referee for helpful remarks about code validation.

This work was supported in part by NASA grants NSG-7416 and NAG-W-710 and by US Department of Energy Grant DE-FG02-85ER53194. A generous grant by Dartmouth College of computer time on the Colorado State University CYBER 205 is gratefully acknowledged. R. B. D. thanks the Astronomy and Physics Department of Dartmouth College for hospitality extended during the preparation of this paper.

REFERENCES

Bateman, G. 1978 *MHD Instabilities*. The MIT Press.

Biskamp, D. 1984 *Phys. Lett.* A **105**, 124.

Bondeson, A. & Sobel, J. R. 1984 *Phys. Fluids* **27**, 2028.

Braginskii, S. I. 1965 Transport processes in a plasma. In *Reviews of Plasma Physics* vol. 1. Consultants Bureau.

Chandrasekhar, S. 1961 *Hydrodynamic and Hydromagnetic Stability*. Clarendon.

Dahlburg, R. B., Zang, T. A., Montgomery, D. & Hussaini, M. Y. 1983 *Proc. Nat. Acad. Sci.* **80**, 5798.

Dahlburg, R. B. 1985 Stability and transition of the driven magnetohydrodynamic sheet pinch. Ph.D. dissertation, College of William and Mary, Williamsburg, VA.

Dungey, J. W. 1958 *Cosmic Electrodynamics*. Cambridge University Press.

Forbes, T. G. & Priest, E. R. 1983 *Solar Phys.* **84**, 169.

Furth, H., Killeen, J. & Rosenbluth, M. N. 1963 *Phys. Fluids* **6**, 459.

Fyfe, D., Montgomery, D. & Joyce, G. 1977 *J. Plasma Phys.* **17**, 369.

Gekelman, W. & Stenzel, R. L. 1981 *J. Geophys. Res.* **86**, 659.

Gekelman, W., Stenzel, R. L. & Wild, N. 1982 *J. Geophys. Res.* **87**, 101.

GOTTLIEB, D. & ORSZAG, S. A. 1977 Numerical analysis of spectral methods: theory and applications. *NSF-CBMS mon.* no. 26, Soc. Ind. App. Math., Philadelphia.

HARLOW, F. H. & WELCH, J. E. 1965 *Phys. Fluids* **8**, 2182.

HERBERT, T. 1983 *J. Fluid Mech.* **126**, 167.

LANDAU, L. D. & LIFSHITZ, E. M. 1959 *Fluid Mechanics.* Pergamon.

MANHEIMER, W. M. & LASHMORE-DAVIES, C. 1984 MHD instabilities in simple plasma configuration. Naval Research Laboratory, Washington DC.

MATTHAEUS, W. H. & MONTGOMERY, D. 1981 *J. Plasma Phys.* **25**, 11.

MATTHAEUS, W. H. 1982 *Geophys. Res. Lett.* **9**, 660.

MATTHAEUS, W. H. & LAMKIN, S. L. 1985 *Phys. Fluids* **28**, 303.

MOIN, P. & KIM, J. 1982 *J. Fluid Mech.* **118**, 341.

MONTGOMERY, D. 1984 Applications of spectral methods to turbulent magnetofluids in space and fusion research. In *Spectral Methods for Partial Differential Equations* (eds. R. G. Voight, D. Gottlieb & M. Y. Hussaini). Soc. Ind. App. Math., Philadelphia.

ORSZAG, S. A. 1971 *J. Fluid Mech.* **50**, 689.

ORSZAG, S. A. & TANG, C.-M. 1979 *J. Fluid Mech.* **90**, 129.

PAO, Y. P., ROSENAU, P. & GUO, S. C. 1983 *Commun. Pure Appl. Maths* **36**, 615.

POUQUET, A. 1978 *J. Fluid Mech.* **88**, 1.

RUTHERFORD, P. H. 1973 *Phys. Fluids* **16**, 1903.

SCHNACK, D. & KILLEEN, J. 1979 *Nucl. Fusion* **19**, 877.

SCHNACK, D. & KILLEEN, J. 1980 *J. Comp. Phys.* **25**, 110.

SONNERUP, B. U. O. 1979 In *Solar System Plasma Physics* (eds. L. Lanzerotti, C. Kennel & E. N. Parker), vol. 3. North Holland.

SOWARD, A. M. & PRIEST, E. R. 1977 *Phil. Trans. R. Soc. Lond.* **284**, 369.

STENZEL, R. L. & GEKELMAN, W. 1981 *J. Geophys. Res.* **86**, 649.

STENZEL, R. L., GEKELMAN, W. & WILD, N. 1982 *J. Geophys. Res.* **87**, 111.

STENZEL, R. L., GEKELMAN, W. & WILD, N. 1983 *J. Geophys. Res.* **88**, 4793.

STUART, J. T. 1958 *J. Fluid Mech.* **4**, 1.

SYROVATSKII, S. I. 1979 *Izv. Akad. Nauk SSSR, Ser. Fiz.* **43**, 695.

VASYLIUNAS, V. M. 1975 *Rev. Geophys. Space Phys.* **13**, 303.

WADDELL, B. V., ROSENBLUTH, M. N., MONTICELLO, D. A. & WHITE, R. B. 1976 *Nucl. Fusion* **16**, 528.

WESSON, J. 1966 *Nucl. Fusion* **6**, 130.

WHITE, R. B., MONTICELLO, D. A., ROSENBLUTH, M. N. & WADDELL, B. V. 1977 *Phys. Fluids* **20**, 800.

WHITE, R. B. 1983 Resistive instabilities and field line reconnection. In *Handbook of Plasma Physics 1* (eds. A. N. Galeev & R. N. Sudan). North Holland.

WILD, N., GEKELMAN, W. & STENZEL, R. L. 1981 *Phys. Rev. Lett.* **46**, 339.